Multiuser Detection in Massive Spatial Modulation MIMO With Low-Resolution ADCs

Shengchu Wang, Yunzhou Li, *Member, IEEE*, and Jing Wang, *Member, IEEE*

***Abstract*—In this paper, we research the multiuser detection (MUD) in a new Spatial Modulation Multiple-Input-Multiple-Output (SM-MIMO) system, whose Base Station (BS) is equipped with massive Radio-Frequency (RF) chains with low-resolution Analog-to-Digital Convertors (ADCs), and the User Equipments (UEs) have multiple Transmit Antennas (TAs) but single RF chain. In the uplink, UEs transmit their data by the Cyclic-Prefix Single-Carrier (CP-SC) SM technique. The key is how to design practical MU detectors to handle the severely quantized measurements and antenna correlations. Coherent detection is focused, so a Least-Square (LS) channel estimator is designed to acquire the the channel side information (CSI) at the Receiver (CSIR). Then, we firstly solve the MUD problem by the Sum-Product-Algorithm (SPA) on a clustered factor graph (FG) whose variable nodes correspond to the transmitted vectors from the UEs. Next, based on the Central Limit Theorem (CLT) and Taylor expansions, the SPA detector (SPAD) is simplified as a new low-complexity Message Passing De-Quantization Detector (MPDQD), which exploits both the structured sparsity and prior probability distribution of the transmitted signal. By utilizing the clustering technique, damping mechanism, and Analog Spatial Filtering (ASF), the robustness of MPDQD is improved significantly. Simulation results show that MPDQD outperforms the linear detectors, works steadily under strong channel correlations, and even performs similarly as its counterpart in the un-quantized SM-MIMO.**

***Index Terms*—Analog spatial filtering, massive MIMO, low-resolution ADC, message passing de-quantization, multiuser detection, spatial modulation, structured sparsity.**

I. Introduction

MASSIVE Spatial Modulation Multiple-Input-Multiple-Output (SM-MIMO) [1]–[6] is a new multiuser (MU) system, where the Base Station (BS) is equipped with massive (N_t) antenna chains, and every User Equipment (UE) has multiple transmit antennas (TAs) but single Radio-Frequency (RF) chain. Through harvesting extremely high MIMO multiplexing and diversity gains [7], the rates, reliability, and power efficiency of the uplink transmission can be improved significantly [3], [8]–[11]. Moreover, by introducing multiple TAs (i.e. additional spatial constellation [12], [13]), the spectral efficiency can be increased without sacrificing the advantages of single-RF chain [2] at the UEs. Finally, hardware implementations of SM-MIMO have been reported in [14]–[16].

However, massive SM-MIMO has a potential drawback that its massive RF chains at the BS could incur high circuit power consumption, which would offset the benefits of "massive" (e.g., the decrease of the transmission power [9], [10]). High circuit-power problem has been noticed in massive MIMO [11], [17], and handled by low-resolution Analog-to-Digital Convertors (ADCs) in our prior works [18], [19]. In this paper, we introduce low-resolution ADCs into massive SM-MIMO to decrease the circuit power consumption at the BS. Similar as [3], the Cyclic-Prefix Single-Carrier (CP-SC) technique [20] is utilized to handle the frequency-selective channels. Finally, we construct a new MU CP-SC massive SM-MIMO system with low-resolution ADCs over frequency-selective channels (called as *massive SM-MIMO* from then on).

However, the new problem is how the BS fulfills the Multiuser Detection (MUD) based on the severely quantized measurements and under the antenna correlations at both the BS and UEs. We focus on the coherent detection, so a Least-Square (LS) channel estimator is proposed to acquire the Channel Side Information at the Receiver (CSIR). For the un-quantized SM-MIMO, there exist bunch of detectors, such as Maximum Likelihood (ML) detector [4], [12], Minimum Mean Square Error (MMSE) detector [12], [13], and message passing detector [3]. But they are not suitable for the quantized massive SM-MIMO due to the following three reasons. Firstly, current detectors failed to consider the quantization effects which cannot be omitted when low-resolution ADCs are used. Secondly, their computational complexities become extraordinarily high due to the curse of dimensionality of massive SM-MIMO (i.e. the numbers of users, BS antennas, and subcarriers are all huge). For example, MMSE has to solve large system of linear equations for every input SC symbol. The message passing detector [3] could be cumbersome because it has to maintain and update a large number of messages. Finally, some of them are not robust to the channel correlations. For example, our numerical results indicate that the performance of MMSE degrades quickly with the increase of the UE antenna correlations.

Consequently, new multiuser detectors have to be constructed for the quantized massive SM-MIMO. In this paper,

Manuscript received June 6, 2014; revised October 15, 2014; accepted December 5, 2014. Date of publication December 18, 2014; date of current version April 7, 2015. This study was supported by National Basic Research Program of China (NO. 2013CB329002), China's 863 Project (NO. 2014AA01A703), National Major Project (NO. 2013ZX03004007), and the Program for New Century Excellent Talents in UniversityNCET-13-0321). Part of this work was presented at IEEE Global Communications Conference (GlobeCom), Austin, TX, USA, December 8–12, 2014. The associate editor coordinating the review of this paper and approving it for publication was W. Gerstacker.

S. Wang is with Electrical Engineering Department and Wireless and Mobile Communications R&D Center, Tsinghua University, Beijing 100084, China (e-mail: wsc11@mails.tsinghua.edu.cn).

Y. Li and J. Wang are with Wireless and Mobile Communications R&D Center, Tsinghua University, Beijing 100084, China (e-mail: liyunzhou@tsinghua.edu.cn; wangj@tsinghua.edu.cn).

Color versions of one or more of the figures in this paper are available online at http://ieeexplore.ieee.org.

Digital Object Identifier 10.1109/TWC.2014.2382098

we firstly solve the MUD problem by the Sum-Product-Algorithm (SPA) on a clustered factor graph (FG) [3], [21]–[23] whose variable nodes correspond to the transmitted vectors from the UEs. However, the SPA detector (SPAD) requires high computational complexity and message passing overhead [24]–[26]. Therefore, it is simplified as a new Message Passing De-Quantization Detector (MPDQD) based on the Central Limit Theorem (CLT) and Taylor expansions [23], [25], [26]. MPDQD has the following four advantages. First, it calls for only matrix-vector multiplication and small-scaled matrix inversions as its most complex operations. Moreover, we show that the matrix inversions can be removed by exploiting the channel correlation statistics. Second, MPDQD exploits both the structured sparsity and prior probability distribution function (pdf) of the transmitted signal. Third, it is quite robust to the quantization losses. Finally, it is also robust to the antenna correlations at the BS and UEs after adopting the clustering technique [21]–[23], damping mechanism [3], [27], and Analog Spatial Filtering (ASF) [28]. Simulation results show that MPDQD outperforms the linear detector and MPDQ [25], and even performs similarly as its counterpart in the un-quantized SM-MIMO. It works steadily even under extremely high channel correlations. In addition, in comparison to massive MIMO [10], [11], massive SM-MIMO shows more superior detection performance, and is more robust to the channel estimation (CE) errors. "To be massive" (making the BS antennas much more than the total TAs of the UEs) is effective to combat with the CSIR errors and quantization losses.

For clarity, our contributions are summarized as follows.

i): We research the multiuser detection in massive SM-MIMO with low-resolution ADCs and over correlated frequency-selective channels. Based on our survey, this has never been discussed.

ii): We develop a low-complexity detector (MPDQD) for the above system. MPDQD is actually a vectorized version of MPDQ [25], and firstly handles the structured-sparse signal reconstruction from the quantized measurements (e.g., a special case is the MUD problem in the quantized SM-MIMO).

iii): We accelerate the matrix-vector multiplications and matrix-inversions in MPDQD, and improve the stability of MPDQD by the damping [3], [27] and ASF [28] techniques. Moreover, a group-wised ASF is proposed to decrease the hardware complexity of the full-scaled ASF.

iv): We construct a new MMSE detector by combining the modified MMSE for the quantized MIMO [29] with the stage-wised MMSE for the un-quantized SM-MIMO [12], [13].

The remainder of this paper is organized as follows. Section II describes the system model of massive SM-MIMO. Section III discusses the CE, and MUD under the CE errors. Section IV develops the stage-wised MMSE detector, and develops two message-passing detectors based on MPDQ [25], and the SPA on a clustered FG. In Section V, MPDQD is constructed. Finally, simulation results are presented in Section VI, and the paper is concluded by Section VII.

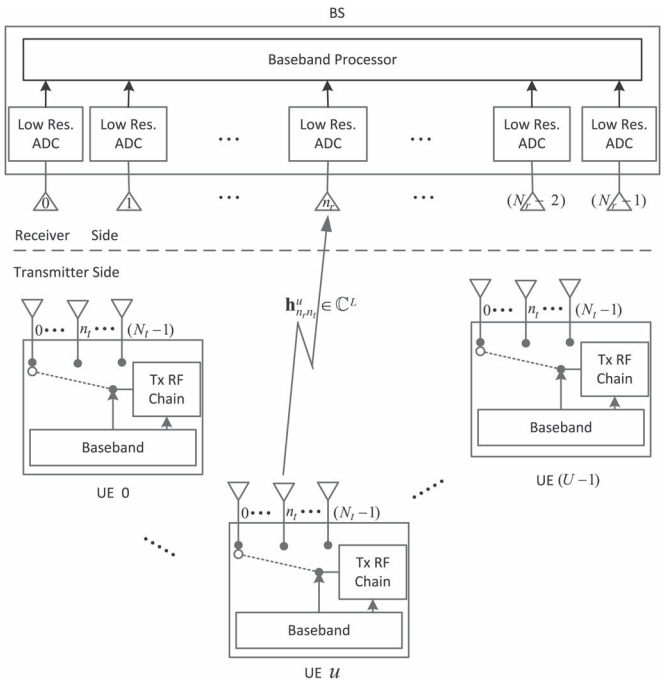

Fig. 1. System configuration of massive SM-MIMO with low-resolution ADCs and over frequency-selective fading channels.

Notation: $[N]=\{0,1,\ldots,N-1\}$ where N is a positive integer. $C\mathcal{N}(\bar{\mu},\bar{\Sigma})$ indicates the complex Gaussian distribution with mean vector $\bar{\mu}$ and covariance matrix $\bar{\Sigma}$. $\mathbf{0}_M$ is an all-zero vector with dimension M, and $\mathbf{0}_{M\times N}$ is an all-zero matrix with size $M\times N$. $\mathbf{I}_N$ is an identity matrix with dimension $N\times N$. For a matrix $\mathbf{B}$, $\mathrm{tr}(\mathbf{B})$ is the trace, B_{mn} is the (m,n)th element, and $\mathbf{B}_{\Omega}$ contains the columns of $\mathbf{B}$ whose indexes come from the integer set Ω. b_n or $\mathbf{b}(n)$ is the nth element of the vector $\mathbf{b}$. $\mathbf{b}^*$ is the component-wise conjugate of $\mathbf{b}$. $\|\mathbf{b}\|_p=\left(\sum_{n=0}^{N-1}|b_n|^p\right)^{1/p}$. $\mathbf{b}_{\Omega}$ contains the entries of $\mathbf{b}$ whose indexes come from Ω. $a:b$ indicates the integers increasing from a to b. $\Re(\cdot)$ and $\Im(\cdot)$ extract the real and imaginary parts of a complex vector or matrix. $\mathrm{mod}(x,y)=x-\lfloor x/y\rfloor y$ where $y\neq 0$ and $\lfloor\cdot\rfloor$ is the flooring function. $(\cdot)^T$ and $(\cdot)^H$ indicate transpose and conjugate transpose, respectively.

II. System Model

In Section II-A, we mainly introduce the system configuration of massive SM-MIMO. Then, the signal transmitting and receiving processes are described in Section II-B and C, respectively.

A. System Configuration of Massive SM-MIMO With Low-Resolution ADCs

Fig. 1 shows the system configuration of massive SM-MIMO. At the transmitter side, there exists U UEs. Every UE has N_t TAs but only one RF chain. At the receiver side, the BS possesses N_r antennas chains with low-resolution ADCs [18], [19]. For $n_r\in[N_r]$, $n_t\in[N_t]$ and $u\in[U]$, $\mathbf{h}^u_{n_rn_t}\in\mathbb{C}^L$ indicates the multipath channel response between the n_rth BS antenna and the n_tth TA of the uth UE, where L is the number of channel taps. $\bar{\mathbf{H}}^u_l\in\mathbb{C}^{N_r\times N_t}$, which contains $\bar{\mathbf{h}}^u_{n_rn_t}(l)$ as the

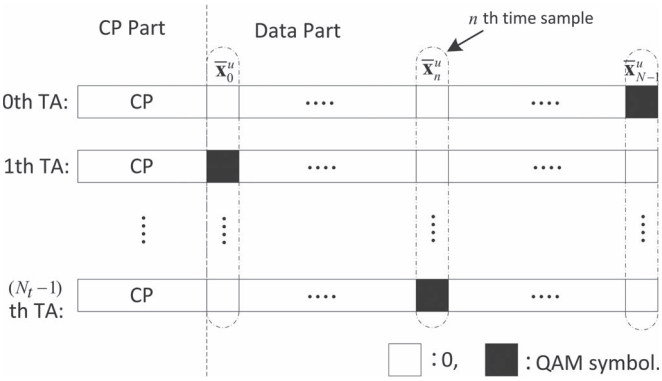

Fig. 2. Example of the SC symbols transmitted by the uth UE; $\bar{\mathbf{x}}_n^u \in \mathbb{C}^{N_t}$ ($n \in [N]$) is the transmitted vector during the nth time sample. Every column hasone and only one non-zero element, so the transmitted signal has structured sparsity.

(n_r, n_t)th element, is the lth MIMO channel tap between the BS and the uth UE. It is modeled as

$$\bar{\mathbf{H}}_l^u = \mathbf{R}_{\text{rx}}^{u\frac{1}{2}} \tilde{\mathbf{H}}_l^u \mathbf{R}_{\text{tx}}^{u\frac{1}{2}} \tag{1}$$

where $\mathbf{R}_{\text{rx}}^u$ and $\mathbf{R}_{\text{tx}}^u$ are the receive and transmit correlation matrices at the uth UE, and $\tilde{\mathbf{H}}_l^u \in \mathbb{C}^{N_r \times N_t}$ is a complex Gaussian matrix with independent and identically distributed (i.i.d.) elements $\sim \mathcal{CN}(0, 1/L)$. In (1), we assume the correlation matrices for the L MIMO channel taps are the same, and $\text{tr}(\mathbf{R}_{\text{rx}}^u) = N_r$ and $\text{tr}(\mathbf{R}_{\text{tx}}^u) = N_t$.

B. Transmitting Operations at the UEs

In the uplink, UEs transmit data-bits to the BS simultaneously through the CP-SC SM technique [20]. Without loss of generality, we only focus on the transmission procedures of the uth UE during one SC symbol. Fig. 2 shows an example of the SC symbols transmitted by the N_t TAs. There, one SC symbol is composed by the CP part and data part which contain L and N time samples, respectively. The CP part is a repetition of the last L time samples of the data part. Therefore, we only focus on the generation of the data part based on the principles of CP-SC SM [20].

Base on [20], the data part can transmit $N\log_2(N_t M)$ data-bits by jointly exploiting the spatial and Quadrature Amplitude Modulation (QAM) constellations of SM [2], [12], [13]. The total data-bits are denoted

$$\mathbf{b}^u = \left[\mathbf{b}_0^u \ \ldots \ \mathbf{b}_n^u \ \ldots \ \mathbf{b}_{N-1}^u\right] \tag{2}$$

where $\mathbf{b}_n^u \in \{0,1\}^{\log_2(N_t M)}$ is a binary row vector. At the $n \in [N]$th time-sample, $\mathbf{b}_n^u$ is extracted from $\mathbf{b}^u$. Its first $\log_2 N_t$ bits is mapped as the index of the chosen active TA (j_n^u), and the remaining $\log_2 M$ bits are mapped as a QAM symbol (q_n^u) belonging to a M-QAM alphabet

$$\mathbb{A} = \left\{\mathbb{I}_{k_R} + i\mathbb{I}_{k_I}, k_R, k_I \in [\sqrt{M}]\right\}. \tag{3}$$

In (3), $\mathbb{I}_k$ is the $k \in [\sqrt{M}]$th element of the Pulse Amplitude Modulation (PAM) alphabet $\mathbb{I} = A \times \{\pm(2c+1), c \in [\sqrt{M}/2]\}$, where M is the QAM modulation order and A is a power normalization factor (e.g., $1/\sqrt{10}$ for 16-QAM). q_n^u will be transmitted by the active TA (i.e., j_n^uth TA). Finally, $\mathbf{b}_n^u$ is mapped as

$$\bar{\mathbf{x}}_n^u = \begin{bmatrix} 0 & \ldots & 0 & \underset{j_n^u\text{th position}}{\overset{q_n^u}{\uparrow}} & 0 & \ldots & 0 \end{bmatrix}^T_{N_t \times 1}, \tag{4}$$

which is the signal vector transmitted by the uth UE at the nth time-sample. Note that silent TAs transmit 0s. All the U UEs can be discussed similar as the uth UE above.

Consequently, by stacking the (4) over u,

$$\bar{\mathbf{x}}_n = \left[\left(\bar{\mathbf{x}}_n^0\right)^T \quad \ldots \quad \left(\bar{\mathbf{x}}_n^u\right)^T \quad \ldots \quad \left(\bar{\mathbf{x}}_n^{U-1}\right)^T\right]^T \tag{5}$$

is formulated as the signal vector transmitted by all the U UEs at nth time-sample. Finally, by assembling the (5) over n together and adding CP, we can obtain

$$\underbrace{\left[\bar{\mathbf{x}}_{N-L} \quad \ldots \quad \bar{\mathbf{x}}_{N-1}\right]}_{\text{CP matrix}} \vdots \underbrace{\bar{\mathbf{x}}_0 \quad \ldots \quad \bar{\mathbf{x}}_n \quad \ldots \quad \bar{\mathbf{x}}_{N-1}}_{\text{Data matrix}} \tag{6}$$

as the signal matrix transmitted by the UN_t TAs of the U UEs during one SC symbol. The $(uN_t + n_t)$th row of (6) is the SC symbol transmitted by the n_tth TA of the uth UE.

C. Receiving Operations at the BS

In this paper, ADC sampling happens at the baseband. After removing CP, at the nth time-sample, the BS receives

$$\bar{\mathbf{y}}_n = Q_c \underbrace{\left(\sum_{l=0}^{L-1} \bar{\mathbf{H}}_l \bar{\mathbf{x}}_{\,\text{mod}\,(n-l,N)} + \bar{\mathbf{w}}_n\right)}_{\bar{\mathbf{z}}_n} \tag{7}$$

where $\bar{\mathbf{z}}_n$ is the signal before quantization, $\bar{\mathbf{H}}_l = [\sqrt{p_s^0}\bar{\mathbf{H}}_l^0 \ \sqrt{p_s^1}\bar{\mathbf{H}}_l^1 \ \ldots \ \sqrt{p_s^{U-1}}\bar{\mathbf{H}}_l^{U-1}]$ is the lth MIMO channel tap between the N_r BS antennas and the U UEs (p_s^u is the signal transmission power of the uth UE), $\bar{\mathbf{w}}_n \sim \mathcal{CN}(\mathbf{0}_{N_r}, \sigma_c^2 \mathbf{I}_{N_r})$ is the complex Gaussian noise with variance σ_c^2. $Q_c(\cdot)$ is a component-wise complex quantizer defined as

$$Q_c(\mathbf{c}) = \left\{Q\left(c_k^R\right) + iQ\left(c_k^I\right)\right\}_{k=0}^{T-1}, \tag{8}$$

where $\mathbf{c} \in \mathbb{C}^T$ is an arbitrary complex vector with $c_k = c_k^R + ic_k^I$ as its kth element, and $Q(\cdot)$ is the midrise b-bit uniform quantizer [30]

$$r = Q(x) = \begin{cases} \text{sign}(x) \cdot \left(\left\lfloor \frac{|x|}{\Delta} \right\rfloor \Delta + \frac{\Delta}{2}\right), & |x| < S + \frac{\Delta}{2}, \\ \text{sign}(x) \cdot S, \text{ otherwise.} \end{cases} \tag{9}$$

where r is the quantization measurement of a real number $x \in \mathbb{R}$, Δ is the quantization step, and $S = (2^{b-1} - 1/2)\Delta$ is the saturation level (ADC saturation happens once $|x| \geq S + \Delta/2$). Note that $Q(\cdot)$ comes from the low-resolution ADCs at the BS.

Furthermore, the upper and lower quantization boundaries of r in (9) can be recovered by a de-quantization operation

$$Q^{-1}(r) = \begin{cases} \left(S - \frac{\Delta}{2}, +\infty\right), & \text{if } r = S \\ \left(-\infty, -S + \frac{\Delta}{2}\right], & \text{if } r = -S \\ \left(r - \frac{\Delta}{2}, r + \frac{\Delta}{2}\right], & \text{otherwise.} \end{cases} \tag{10}$$

By stacking (7) over $n \in [N]$, we have

$$\bar{\mathbf{y}} = Q_c(\underbrace{\bar{\mathbf{H}}\bar{\mathbf{x}} + \bar{\mathbf{w}}}_{\bar{\mathbf{z}}}) \tag{11}$$

where $\bar{\mathbf{y}} = [\bar{\mathbf{y}}_0^T\ \bar{\mathbf{y}}_1^T\ \cdots\ \bar{\mathbf{y}}_{N-1}^T]^T$, $\bar{\mathbf{z}} = [\bar{\mathbf{z}}_0^T\ \bar{\mathbf{z}}_1^T\ \cdots\ \bar{\mathbf{z}}_{N-1}^T]^T$, $\bar{\mathbf{x}} = [\bar{\mathbf{x}}_0^T\ \bar{\mathbf{x}}_1^T\ \cdots\ \bar{\mathbf{x}}_{N-1}^T]^T$, $\bar{\mathbf{w}} = [\bar{\mathbf{w}}_0^T\ \bar{\mathbf{w}}_1^T\ \cdots\ \bar{\mathbf{w}}_{N-1}^T]^T$, and the equivalent channel matrix $\bar{\mathbf{H}} \in \mathbb{C}^{N_r N \times U N_t N}$ is

$$\bar{\mathbf{H}} = \mathrm{TOEP}\left(\left\{\sqrt{p_s^u}\mathbf{h}_{n_r n_t}^u\right\}_{n_r\in[N_r], n_t\in[N_t]}^{u\in[U]}\right) = \begin{bmatrix} \bar{\mathbf{H}}_0 & \mathbf{0} & \cdots & \cdots & \bar{\mathbf{H}}_{L-1} & \cdots & \cdots & \bar{\mathbf{H}}_2 & \bar{\mathbf{H}}_1 \\ \bar{\mathbf{H}}_1 & \bar{\mathbf{H}}_0 & \mathbf{0} & \cdots & \cdots & \cdots & \cdots & \bar{\mathbf{H}}_3 & \bar{\mathbf{H}}_2 \\ \bar{\mathbf{H}}_2 & \bar{\mathbf{H}}_1 & \bar{\mathbf{H}}_0 & \cdots & \cdots & \cdots & \cdots & \mathbf{0} & \bar{\mathbf{H}}_3 \\ \vdots & \vdots & \vdots & \vdots & \vdots & \vdots & \vdots & \vdots & \vdots \\ \mathbf{0} & \cdots & \cdots & \cdots & \cdots & \bar{\mathbf{H}}_{L-1} & \cdots & \bar{\mathbf{H}}_0 & \mathbf{0} \\ \mathbf{0} & \mathbf{0} & \cdots & \cdots & \cdots & \mathbf{0} & \bar{\mathbf{H}}_{L-1} & \cdots & \bar{\mathbf{H}}_0 \end{bmatrix}, \tag{12}$$

where $\mathbf{0}$ is $\mathbf{0}_{N_r \times UN_t}$. During MUD, the Signal-to-Noise Ratio (SNR) is defined as $SNR_{\mathrm{MUD}} = 10\log_{10}(P_s/\sigma_c^2)$ where $P_s = \sum_u p_s^u$.

Finally, we discuss how to determine the quantization step Δ based on (7). Because $Q_c(\cdot)$ is a component-wise operation, we focus on the n_rth elements of $\bar{\mathbf{y}}_n$ and $\bar{\mathbf{z}}_n$, which are denoted as $\bar{y}_n^{n_r}$ and $\bar{z}_n^{n_r}$. In this paper, Δ is chosen to minimize the mean square error (MSE) $E(|\bar{y}_n^{n_r} - \bar{z}_n^{n_r}|^2)$. Based on the channel model (1), $\bar{z}_n^{n_r}$ is a Gaussian random variable $\sim C\mathcal{N}(0, \sum_u r_s^u p_s^u + \sigma_c^2)$, where r_s^u is the square of the l_2-norm of the n_rth row of $\mathbf{R}_{\mathrm{TX}}^{u\,\frac{1}{2}}$. Based on [18], [31], Δ should be set as $\Delta_s = \sqrt{(\sum_u r_s^u p_s^u + \sigma_c^2)/2}\Delta^*$, where Δ^* is the optimal quantization step for the uniform ADC whose input signal is standard Gaussian noise $\sim \mathcal{N}(0,1)$ [31]. For example, Δ^* is 0.3352 for the 4-bit ADC. However, the above strategy could be not optimal. Because the un-quantized measurements $\bar{\mathbf{z}}_n$ are correlated, vector-quantization [30] can be considered to decrease the quantization loss. This is left as our future research topic.

III. Channel Estimation and Multiuser Detection in Massive SM-MIMO

We focus on coherent detection, so the channels $\{\mathbf{h}_{n_r n_t}^u\}_{n_r,n_t}^u$ should be firstly estimated before MUD. In this paper, Least-Square (LS) channel estimator is designed based on the principles of the uplink MU CE in Long-Term Evolution (LTE) [32]. The core idea is: different UEs transmit their own training sequences which are generated by cyclic-shifting a common sequence with different steps, and their channel estimations are separated out in the time domain by the BS.

At the transmitter side, without loss of generality, the uth UE is focused. Its channel training sequence is generated by cyclic right-shifting a common-sequence $\mathbf{t} \in \mathbb{C}^{UK}$ (p_t is the training power, and $\mathbf{t}$ is defined latter) with uK steps ($K \geq L$), and repeating the last L symbols of the shifted sequence as the CP. During the stage of CE, this pilot sequence is transmitted alternatively by the N_t TAs (from the 0th to (N_t-1)th TA) because the UE has only one RF chain [2], [13].

Without loss of generality, we focus on the CE at the n_rth BS antenna after the U UEs have transmitted their training-sequences by their n_tth TAs. After removing CP and based on the basic properties of the circular convolution [7], the received measurements are

$$\mathbf{r}_{n_r} = Q_c\left(\sqrt{p_t}\mathbf{T}\bar{\mathbf{h}}_{n_r n_t} + \mathbf{n}_{n_r}\right) \tag{13}$$

where $\bar{\mathbf{h}}_{n_r n_t} = [(\bar{\mathbf{h}}_{n_r n_t}^0)^T\ (\bar{\mathbf{h}}_{n_r n_t}^1)^T\ \cdots\ (\bar{\mathbf{h}}_{n_r n_t}^{U-1})^T]^T$ with $\bar{\mathbf{h}}_{n_r n_t}^u = [(\mathbf{h}_{n_r n_t}^u)^T\ \mathbf{0}_{(K-L)}^T]^T$, $\mathbf{n}_{n_r} \sim C\mathcal{N}(\mathbf{0}, \sigma_c^2\mathbf{I}_{UK})$ is the noise during CE, and $\mathbf{T}$ is a $UK \times UK$-sized circulant Toeplitz matrix generated from $\mathbf{t}$. The SNR during CE is defined as $SNR_{\mathrm{CE}} = 10\log_{10}(UKp_t/\sigma_c^2)$. Based on Section II-C, the quantization step Δ in (13) is chosen as $\Delta_t = \sqrt{(p_t U + \sigma_c^2)/2}\Delta^*$.

(13) can be transformed as

$$\mathbf{r}_{n_r} = \sqrt{p_t}\mathbf{T}\bar{\mathbf{h}}_{n_r n_t} + \mathbf{n}_{n_r} + \mathbf{n}_{n_r}^q \tag{14}$$

where $\mathbf{n}_{n_r}^q = (\mathbf{r}_{n_r} - \sqrt{p_t}\mathbf{T}\bar{\mathbf{h}}_{n_r n_t} - \mathbf{n}_{n_r})$ is the quantization noise. After treating $\mathbf{n}_{n_r}^q$ as the Gaussian noise $\sim C\mathcal{N}(\mathbf{0}, \Delta_t^2/6\mathbf{I}_{UK})$, the least-square (LS) estimation of $\bar{\mathbf{h}}_{n_r n_t}$ is approximated as

$$\hat{\mathbf{h}}_{n_r n_t} = \frac{1}{\sqrt{p_t}}(\mathbf{T}^H\mathbf{T})^{-1}\mathbf{T}^H\mathbf{r}_{n_r}. \tag{15}$$

Based on [33], $\mathbf{t}$ is designed to satisfy the orthogonality constraint $\mathbf{T}^H\mathbf{T} = UK\mathbf{I}_{UK}$.

Based on the relationship between $\bar{\mathbf{h}}_{n_r n_t}$ and $\mathbf{h}_{n_r n_t}^u$, we know that $\mathbf{h}_{n_r n_t}^u$ can be estimated as the $uK:(uK+L-1)$th entries of $\hat{\mathbf{h}}_{n_r n_t}$, which are denoted as

$$\hat{\mathbf{h}}_{n_r n_t}^u = \mathbf{h}_{n_r n_t}^u + \mathbf{e}_{n_r n_t}^u, \tag{16}$$

where the CE error $\mathbf{e}_{n_r n_t}^u$ is approximately distributed as $C\mathcal{N}(0, \sigma_e^2\mathbf{I}_{UK})$ with $\sigma_e^2 = (\sigma_c^2 + \Delta_t^2/6)/(UKp_t)$. Consequently, in (11), the channel matrix $\bar{\mathbf{H}}$ is approximated as $\hat{\mathbf{H}} = \mathrm{TOEP}(\{\sqrt{p_s^u}\hat{\mathbf{h}}_{n_r n_t}^u\}_{n_r,n_t}^u)$. The CE error matrix is $\mathbf{E} = \mathbf{H} - \hat{\mathbf{H}} = \mathrm{TOEP}(\{-\sqrt{p_s^u}\mathbf{e}_{n_r n_t}^u\}_{n_r,n_t}^u)$. Then, (11) is converted as

$$\bar{\mathbf{y}} = Q_c(\hat{\mathbf{H}}\bar{\mathbf{x}} + \underbrace{\mathbf{E}\bar{\mathbf{x}} + \bar{\mathbf{w}}}_{\hat{\mathbf{w}}}) = Q_c(\underbrace{\hat{\mathbf{H}}\bar{\mathbf{x}} + \hat{\mathbf{w}}}_{\bar{\mathbf{z}}}) \tag{17}$$

$\hat{\mathbf{H}}$ has similar structure as $\bar{\mathbf{H}}$ except replacing $\{\mathbf{H}_l\}_l$ as their estimations $\{\hat{\mathbf{H}}_l\}_l$. Note that $\hat{\mathbf{H}}_l = [\sqrt{p_s^0}\hat{\mathbf{H}}_l^0\ \sqrt{p_s^1}\hat{\mathbf{H}}_l^1\ \cdots\ \sqrt{p_s^{U-1}}\hat{\mathbf{H}}_l^{U-1}]$ where $\hat{\mathbf{H}}_l^u$ contains $\hat{\mathbf{h}}_{n_r n_t}^u(l)$ as its (n_r, n_t)-th element. Based on the statistics of the CE errors, the interference $\mathbf{E}\bar{\mathbf{x}}$ is approximated as Gaussian noise $\sim C\mathcal{N}(\mathbf{0}, L\sigma_e^2 P_s\mathbf{I}_{N_r N})$. Consequently, $\hat{\mathbf{w}} \sim C\mathcal{N}(\mathbf{0}, \hat{\sigma}_c^2\mathbf{I}_{UN_t N})$ where $\hat{\sigma}_c^2 = L\sigma_e^2 P_s + \sigma_c^2$.

In the future, more advanced channel estimators could be developed to handle the quantization effects of the low-resolution ADCs based on the AMP-like algorithms [23], [25], [26]. The inference from CE errors ($\mathbf{E}\bar{\mathbf{x}}$) is actually correlated with the transmitted signal ($\mathbf{x}$). It is simply treated as Gaussian noise in this paper, but could be handled more efficiently by the joint CE and MUD technique [34].

IV. Stage-Wised MMSE Detector and Two Detectors Based on Existing Message Passing Algorithms

In Section III-A, we develop a stage-wised MMSE detector for the quantized SM-MIMO. In Section III-B, two message passing detectors are constructed based on MPDQ [25], and the SPA on a clustered FG [21].

A. Stage-Wised Minimum Mean Square Error Detector

Based on Section II-B,

$$\Omega = \{nUN_t + uN_t + j_n^u\}_{n\in[N],u\in[U]} \tag{18}$$

and the QAM vector $\bar{\mathbf{x}}_\Omega = [q_0^0\ q_0^1\ \cdots\ q_0^{U-1}\ \cdots\ q_{N-1}^0\ q_{N-1}^1\ \cdots\ q_{N-1}^{U-1}]_{UN}^T$ represent the positions and values of the non-zero elements of $\mathbf{x}$, respectively. To recover $\{\mathbf{b}^u\}_{u=0}^U$, Ω and $\mathbf{x}_\Omega$ should be estimated firstly. This problem is solved as follows.

At first, (17) is reformulated as

$$\bar{\mathbf{y}} = \hat{\mathbf{H}}\bar{\mathbf{x}} + \hat{\mathbf{w}} + \hat{\mathbf{w}}^q \tag{19}$$

where $\hat{\mathbf{w}}^q = \bar{\mathbf{y}} - \hat{\mathbf{H}}\bar{\mathbf{x}} - \hat{\mathbf{w}}$ is the quantization noise.

Next, by combining the modified MMSE for the quantized MIMO [29] with the stage-wised MMSE for the un-quantized SM-MIMO [2], [13], a new Minimum Mean Square Error (MMSE) detector is constructed for the quantized massive SM-MIMO. It contains three stages named as *support detection*, *signal reconstruction*, and *bit-stream recovery*, which are designed to estimate the support set Ω, reconstruct the signal vector $\mathbf{x}_\Omega$, and recover the bit-streams $\{\mathbf{b}^u\}_{u=0}^{U-1}$, respectively. Finally, the algorithm details are listed as follows.

i) Support Detection: Firstly, $\bar{\mathbf{x}}$ is estimated as $\hat{\bar{\mathbf{x}}} = G_{\text{MMSE}}\bar{\mathbf{y}}$, where

$$\mathbf{G}_{\text{MMSE}} = \arg\min_{\mathbf{G}} \|\bar{\mathbf{x}} - \mathbf{G}\bar{\mathbf{y}}\|_2^2 \tag{20}$$

is the Minimum Mean Square Error (MMSE) operator. Unfortunately, (20) has no closed-form expression due to the nonlinear quantization operation. A modified MMSE has been constructed for quantized MIMO system in [29]. Similar as [29], after adopting a series of approximations on the second-order statistical relationships between the quantization noise, and the un-quantized and quantized measurements, $\mathbf{G}_{\text{MMSE}}$ is approximated as

$$\mathbf{G}_{\text{MMSE}} \approx \mathbf{R}_{\bar{\mathbf{x}}\bar{\mathbf{x}}}\hat{\mathbf{H}}^H\left((1-\rho_q)\mathbf{R}_{\bar{\mathbf{z}}\bar{\mathbf{z}}} + \rho_q\mathbf{R}_{\bar{\mathbf{z}}\bar{\mathbf{z}}}^D\right)^{-1}, \tag{21}$$

where ρ_q is the distortion factor [29] whose values under different ADC resolutions are tabulated in [31], $\mathbf{R}_{\bar{\mathbf{z}}\bar{\mathbf{z}}} = \hat{\sigma}_c^2\mathbf{I}_{N_rN} + \hat{\mathbf{H}}\mathbf{R}_{\bar{\mathbf{x}}\bar{\mathbf{x}}}\hat{\mathbf{H}}^H$, and $\mathbf{R}_{\bar{\mathbf{z}}\bar{\mathbf{z}}}^D$ is a diagonal matrix containing the main diagonal entries of $\mathbf{R}_{\bar{\mathbf{z}}\bar{\mathbf{z}}}$.

To accelerate the massive matrix inversion in (21), $\mathbf{R}_{\bar{\mathbf{z}}\bar{\mathbf{z}}}^D$ is approximated as $(\hat{\sigma}_c^2 + P_s)\mathbf{I}_{N_rN}$. Based on the above approximation, $\mathbf{R}_{\bar{\mathbf{x}}\bar{\mathbf{x}}} = 1/N_t\mathbf{I}_{UN_tN}$, and the Woodbury identity [35], (21) is simplified as

$$\mathbf{G}_{\text{MMSE}} \approx \left((1-\rho_q)\hat{\mathbf{H}}^H\hat{\mathbf{H}} + \left(\hat{\sigma}_c^2 + \rho_qP_s\right)N_t\mathbf{I}_{UN_tN}\right)^{-1}\hat{\mathbf{H}}^H, \tag{22}$$

which can be decomposed as $NUN_t \times UN_t$ sized matrix-inversions by exploiting the block-Toeplitz structure of $\hat{\mathbf{H}}$.

Secondly, we estimate Ω based on $\hat{\bar{\mathbf{x}}}$. Without loss of generality, we focus on j_n^u. Based on (5) and the structure of $\bar{\mathbf{x}}$ in (11), $\bar{\mathbf{x}}_n^u$ is approximated as $\hat{\bar{\mathbf{x}}}_n^u = \hat{\bar{\mathbf{x}}}(nUN_t + uN_t : nUN_t + uN_t + N_t - 1)$. Then, j_n^u is estimated as $\hat{j}_n^u = \arg\max_{j\in[N_t]}|\hat{\bar{\mathbf{x}}}_n^u(j)|$ as [2], [13].

Consequently, Ω is approximated as

$$\hat{\Omega} = \left\{nUN_t + uN_t + \hat{j}_n^u\right\}_{n\in[N],u\in[U]}. \tag{23}$$

ii) Signal Reconstruction: Based on $\hat{\Omega}$, (19) is shrank as

$$\bar{\mathbf{y}} \approx \hat{\mathbf{H}}_{\hat{\Omega}}\bar{\mathbf{x}}_{\hat{\Omega}} + \bar{\mathbf{w}} + \bar{\mathbf{n}}^q \tag{24}$$

where "$\approx$" appears because $\hat{\Omega}$ could be not equal to Ω precisely.

Similar as (21), the approximated MMSE estimation of $\bar{\mathbf{x}}_{\hat{\Omega}}$ is

$$\hat{\bar{\mathbf{x}}}_{\hat{\Omega}} = \left((1-\rho_q)\hat{\mathbf{H}}_{\hat{\Omega}}^H\hat{\mathbf{H}}_{\hat{\Omega}} + \left(\hat{\sigma}_c^2 + \rho_qP_s\right)\mathbf{I}_{UN}\right)^{-1}\hat{\mathbf{H}}_{\hat{\Omega}}^H\bar{\mathbf{y}} \tag{25}$$

which is the final estimation of $\bar{\mathbf{x}}_\Omega$.

iii) Bit-Stream Recovery: With $u \in [U]$ and $n \in [N]$, j_n^u has been estimated $\hat{j}_n^u$, and q_n^u can be approximated as $\hat{q}_n^u$, which is the QAM hard decision of the $(nU+u)$th entry of $\hat{\bar{\mathbf{x}}}_{\hat{\Omega}}$. At last, the hard decisions of $\{\mathbf{b}^u\}_{u\in[U]}$ can be recovered from $\{\hat{j}_n^u, \hat{q}_n^u\}_{u,n}$ by reverting the SM mapping procedures in Section II-B.

However, the MMSE detector has the following four drawbacks. First, at the stage of *Support Detection*, (22) calls for $NUN_t \times UN_t$ sized matrix-inversions (the block-Toeplitz structure of $\hat{\mathbf{H}}$ has been exploited), which could be problematic in hardware implementation when UN_t is relatively large (e.g., 16 pointed out by [8]). Second, (25) is equivalent to solving large system of linear equations, where $\hat{\mathbf{H}}_{\hat{\Omega}}^H\hat{\mathbf{H}}_{\hat{\Omega}}$ has to be formulated explicitly, and a $UN \times UN$-sized Cholesky decomposition has to be executed. To make matters worse, this cumbersome operation has to be repeated for every input SC symbols because $\Omega(\hat{\Omega})$ would change quickly. Third, MMSE loses its effectiveness once the total number of TAs at the UEs (UN_t) is larger than the number of BS antennas (N_r). Under this case, (11) is under-determined, so (22) fails to provide reliable signal estimation for *support detection*. Fourth, numerical results in Section VI-B show that MMSE is sensitive to the antenna correlations. The second drawback can be circumvented by simply jumping over the stage of *Signal Reconstruction*. However, this incurs performance loss (see Section VI-B), and the simplified MMSE still suffer from the other three drawbacks.

B. MUD Based on Existing Message-Passing Algorithms

In this subsection, we solve the MUD problem in the quantized SM-MIMO by two existing message passing algorithms (i.e., MPDQ [25], and the SPA on a clustered FG [21]).

Firstly, we transform (17) into the real-domain. We define: $\mathbf{y}_n = [\Re(\bar{\mathbf{y}}_n^T)\ \Im(\bar{\mathbf{y}}_n^T)]^T$, $\mathbf{H}_l = [\sqrt{p_s^0}\mathbf{H}_l^0\ \sqrt{p_s^1}\mathbf{H}_l^1\ \cdots\ \sqrt{p_s^{U-1}}\mathbf{H}_l^{U-1}]$ with $\mathbf{H}_l^u = \begin{bmatrix}\Re(\hat{\mathbf{H}}_l^u) & -\Im(\hat{\mathbf{H}}_l^u)\\ \Im(\hat{\mathbf{H}}_l^u) & \Re(\hat{\mathbf{H}}_l^u)\end{bmatrix}$, $\mathbf{x}_n = [(\mathbf{x}_n^0)^T\ \cdots\ (\mathbf{x}_n^u)^T\ \cdots\ (\mathbf{x}_n^{U-1})^T]^T$ with $\mathbf{x}_n^u = [\Re((\bar{\mathbf{x}}_n^u)^T)\ \Im((\bar{\mathbf{x}}_n^u)^T)]^T$, and $\mathbf{w}_n =$

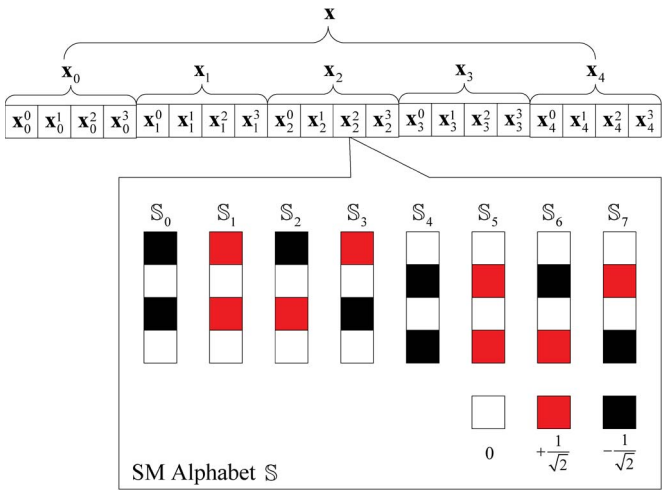

Fig. 3. Structured sparse signal $\mathbf{x}$ under $N=5$, $U=4$, $N_t=2$, and QPSK ($M=4$). It basic unit $\mathbf{x}_n^u$ ($n\in[N]$ and $u\in[U]$) takes values from the SM alphabet $\mathbb{S}$ (show in the box). In $\mathbb{S}$, every element (e.g., $\mathbb{S}_k$ with $k\in[N_tM]$) has only two non-zero elements (red or black blocks) at the same positions of its upper and lower halves.

$[\Re(\hat{\mathbf{w}}_n^T)\ \Im(\hat{\mathbf{w}}_n^T)]^T$ ($\hat{\mathbf{w}}_n$ is a sub-vector containing the $nN_r:((n+1)N_r-1)$-th elements of $\hat{\mathbf{w}}$). Based on the above definitions, (17) is converted as

$$\mathbf{y}=Q(\mathbf{H}\mathbf{x}+\mathbf{w}), \tag{26}$$

where $\mathbf{y}=[\mathbf{y}_0^T\ \mathbf{y}_1^T\ \dots\ \mathbf{y}_{N-1}^T]^T$, $\mathbf{H}$ is constructed by replacing $\{\tilde{\mathbf{H}}_l\}_{l\in[L]}$ in (12) as $\{\mathbf{H}_l\}_{l\in[L]}$, $\mathbf{x}=[\mathbf{x}_0^T\ \mathbf{x}_1^T\ \dots\ \mathbf{x}_{N-1}^T]^T$, $\mathbf{w}=[\mathbf{w}_0^T\ \mathbf{w}_1^T\ \dots\ \mathbf{w}_{N-1}^T]^T$ is the real-valued Gaussian noise with variance $\sigma^2=\hat{\sigma}_c^2/2$.

Consequently, the MUD problem is about how to recover $\mathbf{x}$ based on $\mathbf{y}$. Similar as our previous work [18], it can be solved by MPDQ [25] after treating the entries of $\mathbf{x}$ as i.i.d. random variables distributed as

$$p_X(x)=\left(1-\frac{1}{N_t}\right)\delta(x)+\frac{1}{N_t\sqrt{M}}\sum_{k\in[\sqrt{M}]}\delta(x-\mathbb{I}_k), \tag{27}$$

where $\delta(\cdot)$ is the Dirac function, and $\mathbb{I}_k$ is the kth element of the PAM alphabet $\mathbb{I}$ defined in (3).

Unfortunately, MPDQ has the following two drawbacks which limit its application in SM-MIMO. First, through (27), it has exploited only the sparsity but not the structure sparsity of $\mathbf{x}$. We claim $\mathbf{x}$ has structured sparsity due to the following reasons. Based on the expressions of $\mathbf{x}$ and $\mathbf{x}_n$, one can find that $\{\mathbf{x}_n^u\}_{n\in[N]}^{u\in[U]}$ are the basic units of $\mathbf{x}$. Because $\bar{\mathbf{x}}_n^u$ (4) is a all-zero vector except the M-QAM symbol at the j_n^uth position, and its real and imaginary parts share the same non-zero position j_n^u, $\mathbf{x}_n^u$ has only two non-zero elements at the positions j_n^u and $(N_t+j_n^u)$. Therefore, the non-zero entries of $\mathbf{x}$ are structured organized (see a simple example in Fig. 3). This is quite different to the common sparse signals [25], [36] whose non-zero entries scatter randomly at any positions of the signal vector. So we claim $\mathbf{x}$ is structured sparse signal. Second, MPDQ [25] is sensitive to the UE antenna correlations, under which divergence phenomenon has been observed in Section VI-E (see Fig. 11).

Interestingly, one UE with N_t TAs can be viewed as N_t single-antenna UEs sharing correlated channels. [22], [37], [38] showed that grouping or saying clustering technique was quite useful in designing robust iterative detection algorithms. The core idea is that the signals transmitted from the correlated UEs should be processed as a whole. Therefore, $\mathbf{x}_n^u$ is processed as whole, and treated as a random vector $\sim$

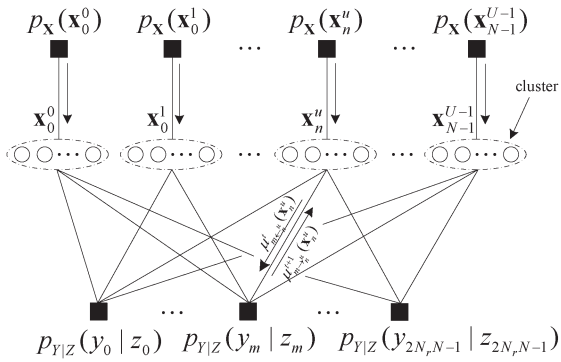

Fig. 4. Factor graph for the MUD problem (26) after clustering $\{\mathbf{x}_n^u\}_{n\in[N]}^{u\in[U]}$ as independent variable nodes (dashed ellipses). Black blocks indicate the factor nodes and solid lines represent the edges between the factor and variable nodes. The bidirectional messages on the edges are given as (30), (31).

$$p_{\mathbf{X}}(\mathbf{x}_n^u)=\frac{1}{N_tM}\sum_{k\in[N_tM]}\delta(\mathbf{x}_n^u-\mathbb{S}_k), \tag{28}$$

where

$$\mathbb{S}_k=\left[0\cdots\underset{\substack{\uparrow\\ j_n^u\text{th position}}}{\Re(\mathbb{A}_m)}\cdots 0\vdots 0\cdots\underset{\substack{\uparrow\\ (N_t+j_n^u)\text{th position}}}{\Im(\mathbb{A}_m)}\cdots 0\right]^T_{2N_t\times 1}$$

is the $k=(j_n^uM+m)$th ($j_n^u\in[N_t]$ and $m\in[M]$) element of the SM alphabet $\mathbb{S}$ (see the example in Fig. 3). Under the terminology of FG [21], $\{\mathbf{x}_n^u\}_{n\in[N]}^{u\in[U]}$ are clustered as independent variable nodes. Then, the MUD problem (26) is described by the FG in Fig. 4. Note clustered FG was proposed by [21], and has been used in the un-quantized SM-MIMO [3]. Here, it is extended to the quantized SM-MIMO by modifying the posterior pdfs $\{p_{Y|Z}(y_m|z_m)\}_{m\in[N_rN]}$ (on the factor nodes) as $\frac{1}{\sqrt{2\pi}\sigma}\int_{t\in Q^{-1}(y_m)}\exp\left(-\frac{(t-z_m)^2}{2\sigma^2}\right)dt$, where y_m and z_m are the mth element of $\mathbf{y}$ and $\mathbf{z}=\mathbf{H}\mathbf{x}$, respectively.

Based on the above clustered FG, SPAD is developed for the quantized massive SM-MIMO as follows. Firstly, the MMSE estimation of $\mathbf{x}_n^u$ is

$$\mathbf{x}_{n,\text{MMSE}}^u=\sum_{\mathbf{x}_n^u\in\mathbb{S}}\mathbf{x}_n^u p_{\mathbf{X}_n^u|\mathbf{Y}}(\mathbf{x}_n^u|\mathbf{y}). \tag{29}$$

Unfortunately, $p_{\mathbf{X}_n^u|\mathbf{Y}}(\mathbf{x}_n^u|\mathbf{y})$ is difficult to be obtained explicitly because high-dimensional summations are needed [21], [23]. Nevertheless, it can be approximately calculated by the SPA iterations:

$$\mu^t_{m\leftarrow_n^u}(\mathbf{x}_n^u)\propto p_{\mathbf{X}}(\mathbf{x}_n^u)\prod_{m'\neq m}\mu^t_{m'\rightarrow_n^u}(\mathbf{x}_n^u) \tag{30}$$

$$\mu^{t+1}_{m\rightarrow_n^u}(\mathbf{x}_n^u)\propto\sum_{\substack{\mathbf{x}_{n'}^{u'}\in\mathbb{S},\\ n'\neq n,u'\neq u}}p_{Y|Z}(y_m|z_m)\prod_{\substack{n'\neq n,\\ u'\neq u}}\mu^t_{m\leftarrow_{n'}^{u'}}\left(\mathbf{x}_{n'}^{u'}\right) \tag{31}$$

$$p^t_{\mathbf{X}_n^u|\mathbf{Y}}(\mathbf{x}_n^u|\mathbf{y})\propto p_{\mathbf{X}}(\mathbf{x}_n^u)\prod_m\mu^t_{m\rightarrow_n^u}(\mathbf{x}_n^u), \tag{32}$$

where the iteration index "t" starts from 0, $\{\mu^0_{m\to{}^u_n}(\cdot)\}^u_{m,n}$ are initialized as 1, "${}^u_n$" represents the variable node $\mathbf{x}^u_n$. After the termination of the SPA iteration (e.g., the maximum iteration number is reached, or the reconstructed signals from two adjacent iterations change slowly), (32) is substituted into (29) to obtain the final estimation of $\mathbf{x}^u_n$.

However, SPAD still involves high-dimensional summations in (31), and has to maintain and update $o(N_rUNL)$ messages, which are rather cumbersome (the message passing detector in [3] has similar problems). Therefore, similar as the stage-wised MMSE detector, SPAD is also not suitable for massive SM-MIMO. Fortunately, a new low-complexity detector (MPDQD) will be developed in the next section.

V. Message Passing De-Quantization Detector for Massive SM-MIMO

This section is the core of this paper. A new message passing de-quantization detector (MPDQD) is developed in Section V-A, and its quick version is given in Section V-B. In Section V-C, damping mechanism and analog spatial filtering are used to improve the stability of MPDQD. Finally, the computational complexity of MPDQD is analyzed in Section V-D.

A. Message Passing De-Quantization Detector

By exploiting the CLT and Taylor expansions [23], [25], [26], SPAD in Section IV can be simplified as a new MPDQD, whose computational complexity is low because it involves matrix-vector multiplications and small-scaled matrix-inversions, and possesses only $o((N_r+U)N)$ messages. The core ideas of the above simplification are rather straightforward. Based on CLT and Taylor expansions, (31) is approximated as a Gaussian function. Consequently, only mean and variance are transformed between variable and factor nodes. Furthermore, based on Taylor expansions, the messages from the one factor (variable) nodes to its connected variable (factor) nodes are not distinguished anymore. So the total number of messages is decreased significantly. Derivation is omitted here due to space constraints. Please refer to [23] and [25] for more details. Finally, the algorithm details of MPDQD are listed as follows.

1) Initialization: Set the iteration index t as 0. For all $m \in [2N_rN]$, $n \in [N]$, and $u \in [U]$, set $\hat{s}_m(-1)=0$, and initialize the mean vector and covariance matrix of $\mathbf{x}^u_n$ as $\hat{\mathbf{x}}^u_n(0)=\mathbf{0}_{2N_t}$ and $\Sigma^{x,u}_n(0)=1/2N_t\mathbf{I}_{2N_t}$, respectively.

2) Iteration: For each $m \in [2N_rN]$, compute:

$$\tau^p_m(t)=\sum_{n,u}\left(\mathbf{h}^u_{mn}\right)^T\Sigma^{x,u}_n(t)\mathbf{h}^u_{mn} \tag{33}$$

where $\left(\mathbf{h}^u_{mn}\right)^T$ is the mth row of the sub-matrix $\mathbf{H}_{2(nU+u)N_t:2(nU+u+1)N_t-1}$, and "$(t)$" indicates the tth iteration.

Calculate:

$$\hat{p}_m(t)=\sum_n\left(\mathbf{h}^u_{mn}\right)^T\hat{x}^u_n(t)-\tau^p_m(t)\hat{s}_m(t-1) \tag{34}$$

$$\hat{s}_m(t)=\frac{1}{\tau^p_m(t)+\sigma^2}\left(\mathrm{E}\left(v_m|v_m\in Q^{-1}(y_m)\right)-\hat{p}_m(t)\right) \tag{35}$$

$$\tau^s_m(t)=\frac{1}{\tau^p_m(t)+\sigma^2}\left(1-\frac{\mathrm{var}\left(v_m|v_m\in Q^{-1}(y_m)\right)}{\tau^p_m(t)+\sigma^2}\right), \tag{36}$$

where the expectation and variance are evaluated with respect to a Gaussian random variables $v_m\sim\mathcal{N}(\hat{p}_m(t),\tau^p_m(t)+\sigma^2)$. $Q^{-1}(\cdot)$ is the de-quantization operation (10).

Compute:

$$\Sigma^{r,u}_n(t)=\left[\sum_m\tau^s_m(t)\mathbf{h}^u_{mn}\left(\mathbf{h}^u_{mn}\right)^T\right]^{-1}. \tag{37}$$

For each pair of $u\in[U]$ and $n\in[N]$, calculate

$$\hat{r}^u_n(t)=\hat{x}^u_n(t)+\Sigma^{r,u}_n(t)\sum\nolimits_m\hat{s}_m(t)\mathbf{h}^u_{mn} \tag{38}$$

$$\hat{x}^u_n(t+1)=\mathrm{E}\left(\mathbf{x}^u_n|\hat{r}^u_n(t),\Sigma^{r,u}_n(t)\right) \tag{39}$$

$$\Sigma^{x,u}_n(t+1)=\mathrm{var}\left(\mathbf{x}^u_n|\hat{r}^u_n(t),\Sigma^{r,u}_n(t)\right). \tag{40}$$

(39) and (40), the mean vector and variance matrix of $\mathbf{x}^u_n$, are evaluated with respect to

$$p\left(\mathbf{x}^u_n|\hat{r}^u_n(t),\Sigma^{r,u}_n(t)\right)\propto\mathcal{N}\left(\mathbf{x}^u_n;\hat{r}^u_n(t),\Sigma^{r,u}_n(t)\right)p_{\mathbf{X}}\left(\mathbf{x}^u_n\right), \tag{41}$$

where $p_{\mathbf{X}}(\mathbf{x}^u_n)$ is the signal prior pdf (28).

3) Termination Judgment: Set $t=t+1$. If the termination condition

$$\frac{\|\hat{x}(t)-\hat{x}(t-1)\|_2}{\|\hat{x}(t)\|_2}\le tol \tag{42}$$

$(\hat{\mathbf{x}}(t)_{2(nU+u)N_t:2(nU+u)N_t-1}$ is $\hat{\mathbf{x}}^u_n(t))$ is satisfied, set $G=t$ (G records the number of iterations before termination), and output $\hat{\mathbf{x}}(G)$ as the final estimation of $\mathbf{x}$; otherwise, go to step 2) for the next iteration.

By substituting (28) into (39)–(41), we have

$$\hat{x}^u_n(t+1)=\sum\nolimits_{k\in[MN_t]}p_k\mathbb{S}_k \tag{43}$$

$$\Sigma^{x,u}_n(t+1)=\sum\nolimits_k p_k\mathbb{S}_k\mathbb{S}_k^T-\hat{x}^u_n(t+1)\left(\hat{x}^u_n(t+1)\right)^T, \tag{44}$$

where $p_k=\phi(\mathbb{S}_k;\hat{\mathbf{r}}^u_n(t),\Sigma^{r,u}_n(t))/P$ with $\phi(\mathbf{s};\mu,\Sigma)=\exp(-1/2(\mathbf{s}-\mu)^T\Sigma^{-1}(\mathbf{s}-\mu))$, and a normalization factor $P=\sum_{k\in[M]}\phi(\mathbb{S}_k;\hat{\mathbf{r}}^u_n(t),\Sigma^{r,u}_n(t))$. Similar as the *Bit-stream Recovery* in MMSE, one can recover the hard-decisions of $\{\mathbf{b}^u\}_{u\in[U]}$ based on $\hat{\mathbf{x}}(G)$ (details are omitted here due to space constraints). Until now, MPDQD is constructed by (33), (44).

MPDQD can be easily extended to the un-quantized system, which can be viewed as a special quantized system with ADC resolution $b\to\infty$ bits. Under the unquantized scenario, the de-quantization function $Q^{-1}(\cdot)$ is degraded as $\delta(\cdot)$. Then, (35), (36) are changed as

$$\hat{s}_m(t)=\frac{y_m-\hat{p}_m(t)}{\tau^p_m(t)+\sigma^2} \tag{45}$$

$$\tau^s_m(t)=\frac{1}{\tau^p_m(t)+\sigma^2}. \tag{46}$$

At the same time, other equations of MPDQD need no modifications.

At last, we briefly comment MPDQD as follows. Firstly, (33)–(41) are routinely obtained by exerting the vectorized SPA-to-AMP simplification [23] on the SPAD (29)–(32). They represent a vectorized version of MPDQ [25], and degrade as (10)–(16) in [25] when the vector size $2N_t$ is 1. Through adjusting the signal prior pdf $p_{\mathbf{X}}(\cdot)$ in (41), they can easily applied

to recover structured-sparse signals (e.g., block-sparse signal with intra-block correlations [39]) from the quantized measurements. In contrast, MPDQ can only handle the classical sparse signals [25], [36]. That is why, compared to MPDQ, MPDQD is more suitable for our MUD problem where the signal to be reconstructed ($\mathbf{x}$) has structured sparsity. This conclusion is further validated by our numerical results in Section VI.

Secondly, $\{\hat{s}_m(t), \tau_m^s(t)\}_{m\in[N_rN]}$ in (35), (36) are the messages on the factor nodes in the lower half of Fig. 4. They are updated based on the messages $\{\hat{\mathbf{x}}_n^u(t), \Sigma_n^{x,u}(t)\}_{n\in[N]}^{u\in[U]}$ from the variable nodes. (39), (40) can be explained similarly. The message updating operations are simple, and involve only two matrix vector multiplications in (34) and (38), and small-scaled matrix inversions in (37). The latter are further accelerated in Section V-B. Different to MPDQ [25], the messages of MPDQD on the variable nodes are mean-vectors and covariance-matrices. This is because MPDQD is simplified from the SPA on a clustered FG whose UN variable nodes indicate $2N_t$-dimensional vectors (i.e. $\{\mathbf{x}_n^u\}_{n\in[N]}^{u\in[U]}$), but MPDQ [25] is simplified from the SPA on the classical FG whose $2UN_tN$ variable nodes represent single variables (i.e. $\{x_k\}_{k\in[2UN_tN]}$, and x_k is the kth entry of $\mathbf{x}$). So the message updating of MPDQD is more complex than that of MPDQ [25]. For example, (33) is much more complex than its counterpart in [25], and (37) involves many $2N_t \times 2N_t$-sized matrix inversions.

Thirdly, similar as the classical Bernoulli-Gaussian sparsity inducing pdf [36], (28) is actually a SM structured sparsity inducing pdf. This point can be intuitively explained as follows. The signal prior pdf (28) is exploited in (39), (40) which are calculated as (43), (44). (43) indicates that the reconstructed $\{\hat{\mathbf{x}}_n^u(t+1)\}_{n\in[N]}^{u\in[U]}$ are prone to peak at $\{\mathbb{S}_k\}_{k\in[N_tM]}$. Therefore, $\hat{\mathbf{x}}(t)$ would have similar structure as $\mathbf{x}$. That is why we say the structured sparsity has been exploited by MPDQD.

Finally, MPDQD takes the influences of the UE antenna correlations into consideration through (37), so it is robust to the latter. In contrast, MPDQ is quite sensitive to the UE antenna correlations. Please refer to Section VI-E for the numerical results.

B. Quick Version of MPDQD

Because even small-scaled matrix-inversions are undesired [8], (37) is simplified by exploiting the channel correlation statistics as follows.

Without loss of generally, we specially consider the uth UE. Based on the structure of $\mathbf{H}$ in (26), $\mathbf{h}_{mn}^u \in \mathbb{R}^{2N_t}$ is either an all-zero vector or the $l \in [L]$th multipath channel tap between the uth UE and the mth BS antenna. In this paper, $\mathbf{h}_{mn}^u(\mathbf{h}_{mn}^u)^T$ is replaced as

$$\mathrm{E}\left(\mathbf{h}_{mn}^u(\mathbf{h}_{mn}^u)^T\right) = \begin{cases} \mathbf{0}_{2N_t\times 2N_t}, & m \notin \Phi_n \\ \mathbf{R}^u, & m \in \Phi_n \end{cases} \tag{47}$$

where Φ_n is the index set of the non-zero rows of the sub-matrix $\mathbf{H}_{2(nU+u)N_t:2(nU+u+1)N_t-1}$, and $\mathbf{R}^u$ is the covariance matrix of the non-zero $\mathbf{h}_{mn}^u$. For example, if $\mathbf{R}_{\mathrm{tx}}^u$ in (1) is real-valued, $\mathbf{R}^u \approx \frac{p_s^u}{2L}\begin{bmatrix} \mathbf{R}_{\mathrm{tx}}^u & \mathbf{0}_{N_t\times N_t} \\ \mathbf{0}_{N_t\times N_t} & \mathbf{R}_{\mathrm{tx}}^u \end{bmatrix} + \frac{p_s^u\sigma_e^2}{2}\mathbf{I}_{2N_t}$.

By substituting (47) into (37), we have

$$\Sigma_n^{r,u}(t) \approx \frac{1}{\sum_{m\in\Phi_n}\tau_m^s}(\mathbf{R}^u)^{-1}. \tag{48}$$

Because the inversion of $\mathbf{R}^u$ can be pre-computed and pre-stored, the matrix-inversions in MPDQD have been removed successfully. Simulation results in Section VI-D show that this quick MPDQD generally performs as well as its original version, and loses its effectiveness only when the BS antennas are strongly correlated with each other. Interestingly, under the i.i.d. case, the above quick-version of MPDQD is exactly the method given in [1].

C. Increasing the Stability of MPDQD by Damping and ASF

MPDQD could diverge due to the aggressive message updating in (39) and (40), and the correlations among the BS measurements. The first type of divergence can be solved by the well-known damping technique [3], [27] which changes (39) and (40) as

$$\begin{aligned} \hat{x}_n^u(t+1) &= \lambda\hat{x}_n^u(t) + (1-\lambda)\mathrm{EXP}\left(\mathbf{x}_n^u|\hat{r}_n^u(t), \Sigma_n^{r,u}(t)\right) \\ \Sigma_n^{x,u}(t+1) &= \lambda\Sigma_n^{x,u}(t) + (1-\lambda)\mathrm{VAR}\left(\mathbf{x}_n^u|\hat{r}_n^u(t), \Sigma_n^{r,u}(t)\right). \end{aligned}$$

where $\lambda \geq 0$ is a damping parameter.

In this paper, we deal the second divergence by de-correlating the BS measurements through ASF [28]. Without loss of generality, we focus on the $n \in [N]$th time-sample. $\bar{\mathbf{z}}_n \in \mathbb{C}^{N_r}$ in (7) is the measurement vector before ADC sampling. Due to the antenna correlation at the BS, its entries are not independent, and their covariance matrix is $\mathbf{R}_{\bar{\mathbf{z}}_n\bar{\mathbf{z}}_n} = \mathrm{E}_{\mathbf{x},\mathbf{H}}(\bar{\mathbf{z}}_n\bar{\mathbf{z}}_n^T)$, which is approximated as

$$\mathbf{R}_{\bar{\mathbf{z}}_n\bar{\mathbf{z}}_n} \approx \mathbf{R}_{\bar{\mathbf{z}}\bar{\mathbf{z}}} = \sum\nolimits_{u\in[U]} p_s^u\mathbf{R}_{\mathrm{rx}}^u + \sigma_c^2\mathbf{I}_{N_r}. \tag{49}$$

after omitting the inter-column correlations in $\mathbf{H}$. Therefore, $\bar{\mathbf{y}}_n = Q_c(\bar{\mathbf{z}}_n)$ in (7) is also a correlated vector, so is $\mathbf{y}$ in (26). Consequently, the messages output from the factor nodes in the lower half of Fig. 4 are correlated with each other. This causes the instabilities of the message passing algorithms (e.g., divergence of MPDQ is observed in Section VI-E). For the above instability problem, one potential solution is de-correlating the factor nodes, which is achieved by exerting ASF on the $\bar{\mathbf{z}}_n$ as follows.

Firstly, we calculate the singular value decomposition (SVD) of $\mathbf{R}_{\bar{\mathbf{z}}\bar{\mathbf{z}}}$ as $\mathbf{Q}\Lambda\mathbf{Q}^H$, where $\mathbf{Q}$ is a unitary matrix and Λ is a diagonal matrix. Then, by left-multiplying $\mathbf{Q}^H$ with $\bar{\mathbf{z}}_n$, we obtain a new measurement vector

$$\tilde{\mathbf{z}}_n = \mathbf{Q}^H\bar{\mathbf{z}}_n \tag{50}$$

whose covariance matrix is defined as $\mathbf{R}_{\tilde{\mathbf{z}}_n\tilde{\mathbf{z}}_n} = \mathrm{E}_{\mathbf{x},\mathbf{H}}(\tilde{\mathbf{z}}_n\tilde{\mathbf{z}}_n^T)$, and can be approximated as Λ. Therefore, $\tilde{\mathbf{z}}_n$ is an approximately un-correlated vector, so is the new quantized measurement vector $\tilde{\mathbf{y}}_n = Q_c(\tilde{\mathbf{z}}_n)$. Because $\bar{\mathbf{z}}_n$ corresponds to the analog signal before ADC quantization, the matrix-vector multiplication in (50) has to be implemented in the analog domain, and is exactly the ASF operation in [28]. After ASF, the MUD will be executed as follows. (17) is modified by replacing $\bar{\mathbf{y}}_n$ as $\tilde{\mathbf{y}}_n$, and $\hat{\mathbf{H}}_l$ as $\mathbf{Q}\hat{\mathbf{H}}_l$. Then, the modified equation is transformed into the real domain as (26). Finally, MPDQD is executed to

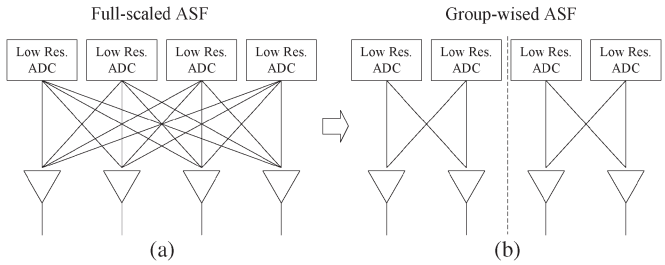

Fig. 5. (a) Full-scaled ASF [28]. (b) Group-wised ASF. Every line implicitly contains a phase shifter and Variable Gain Amplifier (VGA).

TABLE I
COMPLEXITIES OF THE MOST COMPUTATION-INTENSIVE STEPS AMONG MPDQD AND MMSE

MPDQD	(33)	(34) and (38)	(37)
flops	$o(LNUN_rN_t^2)$	$o(NUN_tN_r)$	$o(LNUN_rN_t^2)$
MMSE	(22)	(25)	–
flops	$o(NU^3N_t^3)$	$o(LN^2N_rU^2+U^3N^3)$	–

recover $\mathbf{x}$. Simulation results in Section VI-E validate that, after adopting ASF (50), MPDQD can work steadily even when the BS antennas are strongly correlated with each other.

However, the above ASF scheme requires a $N_r \times N_r$-sized analog beamforming (BF) network, which is composed by phase shifters and variable gain amplifiers (VGAs) [28]. Because N_r is as large as hundreds [10], [11], ASF incurs high hardware cost and energy consumption, which will partially offset the benefits from adopting low-resolution ADCs. Considering this, we propose a group-wised ASF design. The basic idea is simple. The N_r BS antennas are uniformly divided into K groups, and every group contains $N_r^g = N_r/K$ antennas (for clarity, we assume $\mathrm{mod}\,(N_r,K)=0$). Then, the inter-group antenna correlations are omitted, and the intra-group correlations are diminished by K parallel small-scaled ASF networks. A simple example is given in Fig. 5.

Mathematically, we firstly approximate $\mathbf{R}_{\bar{\mathbf{z}}\bar{\mathbf{z}}}$ as a block-diagonal matrix $\hat{\mathbf{R}}_{\bar{\mathbf{z}}\bar{\mathbf{z}}}$ after retaining only the $kN_r^g:[(k+1)N_r^g-1]$-th (with $k\in[K]$) rows and columns of $\mathbf{R}_{\bar{\mathbf{z}}\bar{\mathbf{z}}}$. Then, the SVD of $\hat{\mathbf{R}}_{\bar{\mathbf{z}}\bar{\mathbf{z}}}$ is calculated as $\hat{\mathbf{Q}}\hat{\Lambda}\hat{\mathbf{Q}}^H$. Finally, $\hat{\mathbf{Q}}$, which is also a block-diagonal matrix, is applied into ASF. Therefore, only $KN_r^g \times N_r^g$-sized analog BF networks are required. Compared to the original $N_r \times N_r$-sized one, they call for $(1-1/K)N_r^2$ less phase-shifters and VGAs. So the corresponding hardware cost and energy consumption can be decreased significantly especially when K is large (i.e. N_r^g is small). Our numerical results in Section VI-E indicate that, when $N_r^g = 8$, MPDQD with group-sized ASF reaches similar convergence performance as the full-scaled case. Finally, once the correlation matrix (49) is changed, the coefficients of ASF must be adjusted correspondingly. Fortunately, they could be kept constant in a long time period, because (49) is usually changed slowly [40].

D. Computational Complexity of MPDQD

Based on Table I, the total computational complexity of MPDQD is $o(G(NUN_rN_t+LNUN_rN_t^2))$, where G is the number of iterations before MPDQD is terminated (i.e. (42) is satisfied). Based on [25], [26], the convergence speed of the AMP-like algorithms (including MPDQD) are irrelevant to the problem dimensions. So, once $\alpha = U/N_r$ is fixed, G keeps almost unchanged no matter how large U and N_r are. Therefore, the complexity of MPDQD is with the order $o(NUN_tN_r + LNUN_rN_t^2)$. Based on [19], [25], the complexity of MPDQ is $o(NUN_tN_r)$, which is lower than that of MPDQD. Finally, the complexity of MMSE is $o(NU^3N_t^3+LN^2N_rU^2+U^3N^3)$, which is much higher than that of both MPDQD and MPDQ.

VI. SIMULATION

For clarity, the common system parameters are summarized as follows. The ADC resolution is fixed as $b=4$ bits. In one SC symbol, the data length is $N=128$, and the CP length is $L=20$ which is equal to the number of channel taps. The termination parameters in (42) is $tol = 10^{-3}$. The channel correlation matrices in (1) are generated as $\mathbf{R}_{\mathrm{tx}}^u = \mathrm{R}(\rho_{\mathrm{UE}},N_t)$ and $\mathbf{R}_{\mathrm{rx}}^u = \mathrm{R}(\rho_{\mathrm{BS}},N_t)$, where ρ_{BS} and ρ_{UE} are the common correlation coefficients for all the U UE, and the operator $\mathrm{R}(\rho,N)$ formulates a $N\times N$-sized matrix whose (m,n)th element is $\rho^{|m-n|}$ (0^0 is defined as 1). Without special note, full-scaled ASF is always adopted in MPDQD when ρ_{BS} is non-zero. The noise variance σ_c^2 is fixed as 1, and the signal transmission powers $(\{p_s^u\}_{u\in[U]})$ are the same as p_s, i.e. all the U UEs transmit signals with the same power. During the CE in Section III, K is fixed as $2L$. The BERs are obtained by averaging across all the U UEs. The the damping parameter λ is fixed as 0.3.

A. Robustness of MPDQD to the Channel Estimation Errors and Quantization Losses

MPDQD is tested under three types of CSIRs, i.e. oracle CSIR ("oral. CSIR"), and the CSIRs acquired by the LS estimator under two SNR_{CE}s (i.e. 20 and 25 dB). The BER lower bound is provided by MPDQD in the un-quantized SM-MIMO. Fixed system parameters are: $N_r=128$, $N_t=4$, and 16-QAM. U is varied as 16 and 48, which correspond to two interesting cases that $UN_t < N_r$ and $UN_t > N_r$.

Fig. 6 provides two important observations. Firstly, under different CSI precisions, MPDQD still successfully approaches to its lower bound (black curves). The performance gaps are especially small if the "massive" condition (i.e. $N_r \gg UN_t$) is satisfied (e.g., $U=16$). For example, when $SNR_{\mathrm{CE}} = 25$ dB, at BER 10^{-2}, the SNR gap is 2.5 dB when U is 48, and decreased as 0.4 dB when U is 16. Under the oracle CSI case, the performance gap between MPDQD and its lower bound are caused only by the 4-bit quantization losses. Surprisingly, its value is very small. For example, compared to the lower bound, MPDQD shows only $0\sim 0.6$ ($0\sim 2$) dB performance losses when U is 16 (48). In summary, MPDQD is robust to the quantization losses, and "to be massive" is effective to combat with both the CE errors and the quantization noises (a special type of hardware imperfection). The latter is a famous conclusion in massive MIMO [10], [11], and observed again in massive SM-MIMO.

Secondly, the detection performance of MPDQD strongly relies on the CSI quality. Fig. 6 shows that, with the increase of the CSI precision, detection performances of MPDQD is gradually improved. Fortunately, when SNR_{CE} is moderately high

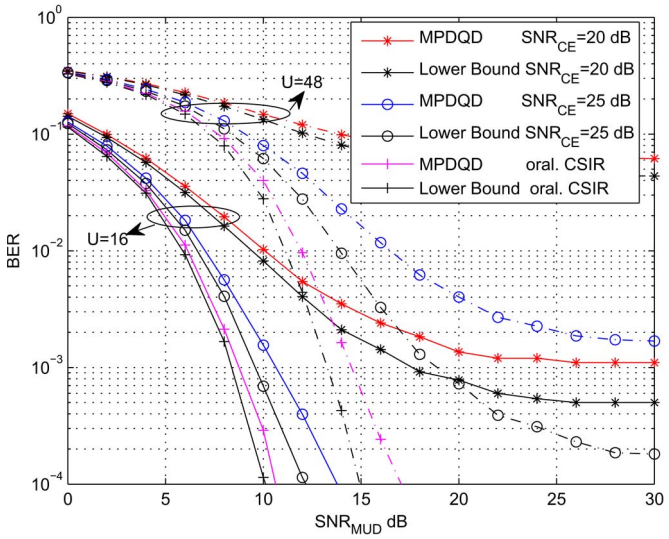

Fig. 6. BER performance of MPDQD under different CSIR accuracies. "Lower Bound" is provided by MPDQD in the un-quantized SM-MIMO. SNR_{CE} is varied as 20 and 25 dB, and "Oral. CSIR" means CSIR is precisely known by the BS. $\rho_{\text{BS}} = 0.5$, $\rho_{\text{UE}} = 0.3$, $b = 4$ bits, $N_r = 128$, $N_t = 4$, and 16-QAM. U is varied as 16 (solid lines) and 48 (dash lines) which correspond to $UN_t < N_r$ and $UN_t > N_r$, respectively.

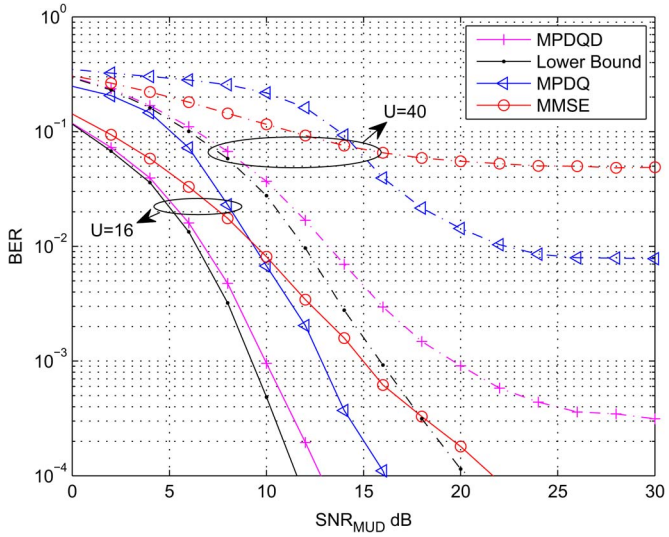

Fig. 7. BER performances of MPDQD, MPDQ and MMSE over the i.i.d. channels ($\rho_{\text{BS}} = \rho_{\text{UE}} = 0$). "Lower Bound" is provided by MPDQD in the un-quantized SM-MIMO. $SNR_{\text{CE}} = 25$ dB, $b = 4$ bits, $N_r = 128$, $N_t = 4$, and 16-QAM. U is varied as 16 (solid lines) and 40 (dashed lines) which correspond to $UN_t < N_r$ and $UN_t > N_r$, respectively.

(e.g., 25 dB), the performance lose caused by the CSI errors could be acceptable. For example, we consider $SNR_{\text{CE}} = 25$ dB and BER 10^{-2}. When U is 16 (48), the SNR loss of MPDQD is 0.9 (4.5) dB compared to the oracle CSI case. Consequently, the CE errors are not the bottleneck of massive SM-MIMO with $N_r \gg UN_t$ and relatively high SNR_{CE}. Note that high SNR_{CE} can be reached by increasing the transmission power p_t or emitting longer training sequences. In the future, channel sparsity [41] could be exploited to decrease the consumption of the training resources.

B. MPDQD v.s. MMSE and MPDQ

In the first experiment, we consider the i.i.d. case (i.e. $\rho_{\text{BS}} = 0$ and $\rho_{\text{UE}} = 0$). The fixed parameters are: $SNR_{\text{CE}} = 25$ dB, $N_r = 128$, $N_t = 4$, and 16-QAM. U is varied as 16 and 40, which correspond to $UN_t < N_r$ and $UN_t > N_r$, respectively. Fig. 7 shows that MPDQD outperforms both MPDQ and MMSE significantly. When $U = 16$, MPDQD shows about 3 dB gains over MPDQ. Compared to MMSE, its performance gain keeps increasing with the increase of SNR_{MUD}. For example, the gain is 2.7 dB at BER 10^{-2}, and 5 dB at BER 10^{-3}. The performance gains of MPDQD over both MPDQ and MMSE becomes more apparent when U is increased as 40. Actually, when $N_r < UN_t$, MMSE almost loses its effectiveness, and stuck at a high "error floor" $10^{-1.3}$ once SNR_{MUD} exceeds 15 dB. This is because (19) is under-determined, and (22) fails to provide reliable signal estimation for *support detection*. In contrast, by exploiting the sparsity of the transmitted signal $\mathbf{x}$ in (26), MPDQ outperforms MMSE, but still shows a high "error floor" at BER $10^{-2.1}$. In contrast, MPDQD beats the previous two detectors. At BER 10^{-2}, it has 9 dB SNR gain over MPDQ, which should attribute to the successful exploitation of the structured sparsity of $\mathbf{x}$ (see Section V-A for more details). Due to the CE errors and quantization losses, MPDQD also shows "error floor" at BER $10^{-3.5}$. Interestingly, under the case of $U = 16(N_r > UN_t)$, MPDQD has only $0 \sim 1.5$ dB SNR loss compared with its lower bound. Similar as Section VI-A, this observation further validates the power of "massive" in combating with the CE errors and quantization losses.

In the second experiment, we discuss how different detectors are influenced by the antenna correlations at the UE side. MPDQD and MMSE are used. A simplified MMSE ("simp. MMSE") is also considered. It is obtained after jumping over the stage of *signal reconstruction* in MMSE, and has much lower complexity (refer to Section III-A for more details). MPDQ is not used because it could diverge (see Section VI-E). Fixed parameters are: $\rho_{\text{BS}} = 0.5$, $SNR_{\text{CE}} = 25$ dB, $N_r = 196$, $U = 16$, $N_t = 4$, and 16-QAM. Fig. 8 provides three important observations. First, compared to MMSE and "simp. MMSE", MPDQD is more robust to antenna correlations. For example, when ρ_{UE} is increased from 0.3 to 0.7, the SNR loss of MPDQD is 1.2 (3.5) dB at BER 10^{-2} (10^{-3}). In contrast, at BER 10^{-2}, MMSE and "simp. MMSE" show 3 and 4.5 dB SNR loss, respectively. MMSE shows 10.5 dB losses at BER 10^{-3}, and "simp. MMSE" failed to reach the BER 10^{-3}. Second, MPDQD can approach its performance lower bound even when there exist antenna correlations at the UE side. Third, MMSE outperforms "simp. MMSE", and its performance gain is more apparent when the UE antenna correlation is high. For example, at BER 10^{-2}, the SNR advantage is enlarged from 1.5 dB to 5 dB when ρ_{UE} is increased from 0.3 to 0.7.

C. Spatial Modulation or Not?

[3] validated that SM-MIMO outperformed the classical MU-MIMO system [7]. However, [3] focused on the un-quantized case, perfect CSI, and i.i.d. channels. A natural question is: whether the advantages of SM can still be kept under the low-resolution quantization, imperfect CSI, and channel correlation in our paper? To answer this question, the

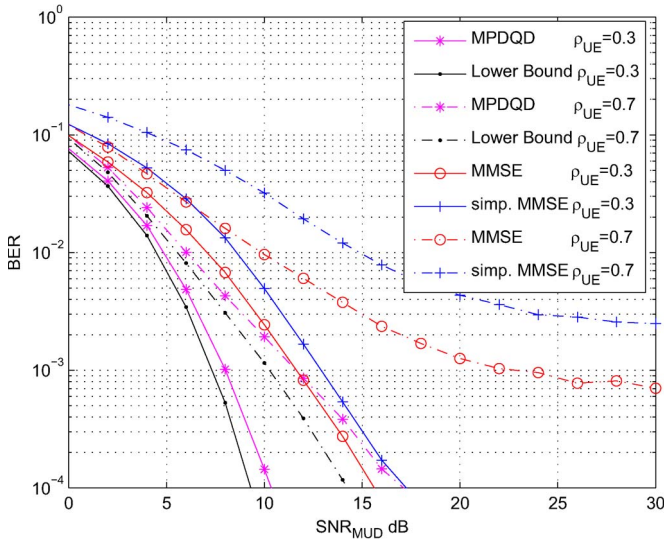

Fig. 8. Robustness to the UE antenna correlations (ρ_{UE} is varied as 0.3 and 0.7, which correspond to weak and strong antenna correlations). $\rho_{\text{BS}} = 0.4$, $SNR_{\text{CE}} = 25$ dB, $b = 4$ bits, $N_r = 192$, $U = 16$, $N_t = 4$ and 16-QAM.

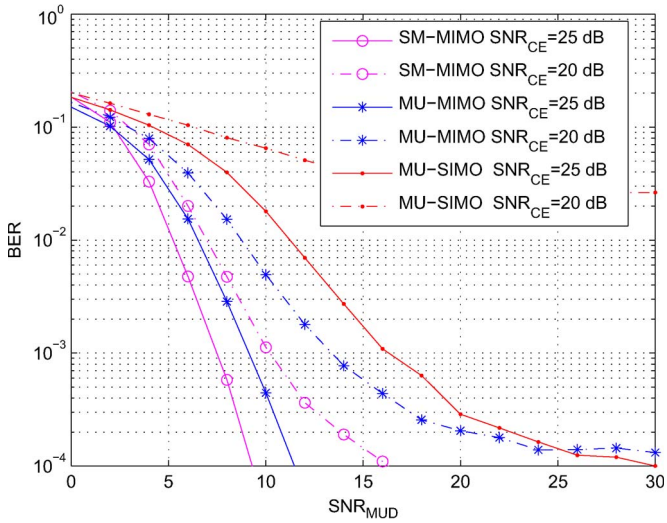

Fig. 9. SM-MIMO with $N_t = 4$ and QPSK, v.s. two MU MIMOs [7] (i.e. "MU-SIMO" with $N_t = 1$ and 16-QAM, and "MU-MIMO" with $N_t = 2$ and QPSK). $\rho_{\text{BS}} = \rho_{\text{UE}} = 0.4$, $b = 4$ bits, $N_r = 120$, and $U = 32$.

following experiment is designed. Under the same system throughput $4U$ bits-per-channel-usage (bpcu), SM-MIMO with $\{N_t = 4, \text{QPSK}\}$ is compared to two classical MU MIMOs [7] with $\{N_t = 1,\ 16\text{-QAM}\}$ and $\{N_t = 2,\ \text{QPSK}\}$, respectively. The latter two are named as "MU-SIMO" and "MU-MIMO" based on whether the UE has single RF chain (i.e. whether N_t is 1). The fixed parameters are: $U = 32$, $N_r = 120$, $\rho_{\text{BS}} = 0.4$, and $\rho_{\text{UE}} = 0.4$. MPDQD is extended to the MU-MIMO case by simply adjusting the signal prior pdf $p_{\mathbf{X}}(\cdot)$ in (41).

Fig. 9 shows that SM-MIMO outperforms the two MU-MIMOs. For example, when SNR_{CE} is 25 dB, compared to "MU-SIMO" and "MU-MIMO", its performance gains are 1.3 and 6 dB at BER 10^{-2}, respectively. With the decrease of SNR_{CE} (i.e. the CSI precision), the BER performances of the two MU-MIMOs degrades much more quickly than that of SM-MIMO. For example, when SNR_{CE} is decreased from 25 dB to

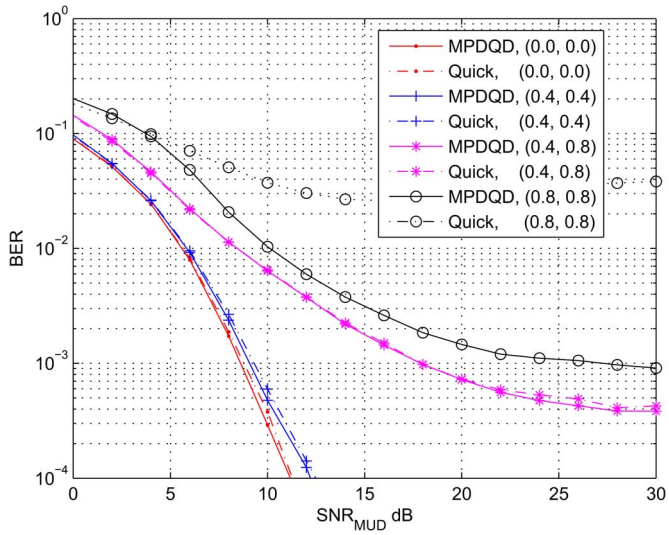

Fig. 10. MPDQD (solid curves) versus its quick version (dash curves) under different degrees of antenna correlations at the BS and UEs. Numbers in the legend indicate different $(\rho_{\text{BS}}, \rho_{\text{UE}})$s. $SNR_{\text{CE}} = 25$ dB, $b = 4$ bits, $N_r = 160$, $U = 16$, $N_t = 4$ and 16-QAM.

20 dB, at BER 10^{-3} (10^{-2}), the SNR loss of SM-MIMO is 2.5 (1.7) dB, and the SNR loss of "MU-MIMO" is 4.5 (2.2) dB; the "error floor" of "MU-SIMO" is quickly raised from 10^{-4} to $10^{-1.6}$. In summary, compared to the classical MU-MIMO [7], SM-MIMO shows more superior detection performance, and is more robust to CE errors. The latter phenomenon has been observed in the un-quantized SM-MIMO over the flat-fading channels [42], [43].

D. MPDQD v.s. Its Quick Version

In this part, MPDQD is compared to its quick version introduced in Section V-B. Fixed parameters are: $N_r = 128$, $U = 32$. Fig. 10 indicates that the quick algorithm approaches to the performance of MPDQD when the BS antenna correlation is relatively weak (e.g., $\rho_{\text{BS}} = 0.4$ in the "+" and "*" lines). This conclusion exists even when the UE antenna correlation is extremely high ($\rho_{\text{UE}} = 0.8$ in the star lines). But the quick MPDQD diverges when the BS antenna correlation is strong (e.g., $\rho_{\text{BS}} = 0.8$ in the circle lines). The effectiveness of the quicken method is also validated under the i.i.d. case (point lines) for which more simulations results can be found in [1]. In the future, we would develop quick MPDQD under extremely strong antenna correlation at the BS.

E. Convergence Performance

Both ρ_{BS} and ρ_{UE} are increased from 0 to 0.9. Under different values of $\{\rho_{\text{BS}}, \rho_{\text{UE}}\}$, MPDQ and MPDQD are executed 500 times. Their maximum numbers of iterations are limited as 50. "Divergence" is claimed to happen if the final reconstructed signal is not better than the initial all-zero vector, or signal recovery at some specified iteration becomes numerically unstable, i.e. NAN ("Not A Number") is detected during the Matlab simulations.

Fig. 11 provides two important observations. Firstly, clustering technique ensures MPDQD is robust to the antenna

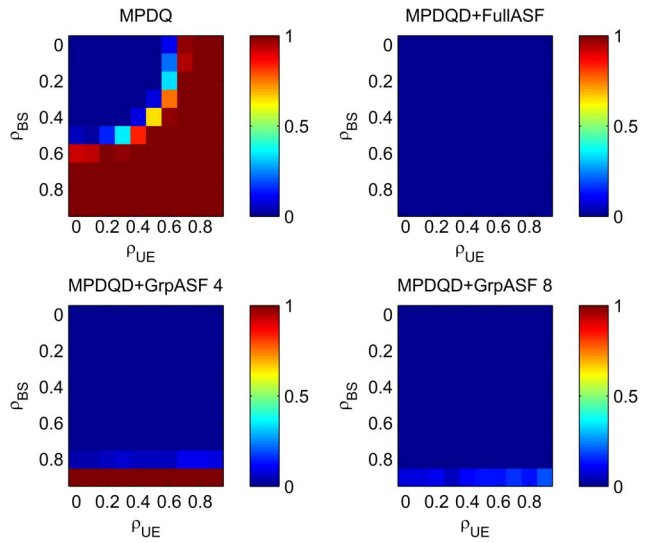

Fig. 11. Divergence probabilities of MPDQ and MPDQD under different different degrees of antenna correlations at the BS and UEs (i.e. different ρ_{UE}s and ρ_{BS}s). Their values are indicated by different colors. "FullASF" means the full-scaled ASF, and "GrpASF #" indicates group-wised ASF with the group-size $N_r^{\text{g}} = \#$. $SNR_{\text{MUD}} = 5$ dB, $SNR_{\text{CE}} = 25$ dB, $b = 4$ bits, $N_r = 128$, $U = 16$, $N_t = 4$ and 16-QAM.

correlations at the UE side. When $\rho_{\text{BS}} = 0$, divergence of MPDQ appears once ρ_{UE} exceeds 0.5, and happen with probability 1 once ρ_{UE} is larger than 0.75. In contrast, MPDQD can converge safely even when the antenna correlation at the UE side is extremely strong (e.g., $\rho_{\text{UE}} = 0.9$). This is because MPDQD specially considers the channel correlations in (37)–(40).

Secondly, ASF ensures MPDQD to be robust to the antenna correlations at the BS. Moreover, the proposed group-wised ASF could be as effective as the full-scaled one [28], and its hardware complexity is much lower than the latter (see Section V-C). Fig. 11 indicates that, even when the group-size N_r^g is as small as 4, MPDQD can converge with probability 1 except when the BS antenna correlation is extremely strong (e.g., $\rho_{\text{BS}} = 0.9$). When N_r^g is increased as 8, even when ρ_{BS} is as large as 0.9, divergence still happens with very small probability $0.01 \sim 0.056$.

VII. Conclusion

In this paper, we proposed a low-complexity Message Passing De-Quantization Detector (MPDQD) for massive spatial modulation MIMO system with low-resolution ADCs and over frequency-selective channels. MPDQD can exploit both the structured sparsity and prior probability distribution of the transmitted signals. It relies on the clustering technique and analog spatial filtering to handle the antenna correlations at the transmitter and receiver side. Simulation results validate that MPDQD significantly outperforms the linear detector, successfully offsets the quantization effects from the low-resolution ADCs, and works steadily even under strong antenna correlations. Compared to classical massive MIMO systems, massive SM-MIMO is more robust to channel estimation errors. In the future, MPDQD should be tested under more practical channel models.

Acknowledgment

The authors thank both the editor and anonymous reviewers for their insightful comments which have helped us to improve the quality of this paper. Shengchu Wang thanks Dr. Ulugbek S. Kamilov for his warmhearted helps on learning the paper [25].

References

[1] S. C. Wang, Y. Z. Li, J. Wang, and X. Xu, "Multiuser detection in massive spatial modulation (SM-) MIMO with low-resolution ADCs," in *Proc. IEEE GlobeCom*, 2014, to be published.

[2] M. D. Renzo, H. Haas, A. Ghrayeb, S. Sugiura, and L. Hanzo, "Generalized MIMO: Challenges, opportunities, and implementation," *Proc. IEEE*, vol. 102, no. 1, pp. 56–103, Jan. 2014.

[3] P. Raviteja, T. L. Narasimhan, and A. Chockalingam, "Large-scale multiuser SM-MIMO versus massive MIMO," in *Proc. ITA*, San Diego, CA, USA, Feb. 2014, pp. 1–9.

[4] N. Serafimovski1, S. Sinanovic, M. D. Renzo, and H. Haas, "Multiple access spatial modulation," *EURASIP J. Wireless Commun. Netw.*, vol. 2012, p. 299, Sep. 2012.

[5] M. Di Renzo and H. Haas, "Bit error probability of space-shift keying MIMO over multiple-access independent fading channels," *IEEE Trans. Veh. Technol.*, vol. 60, no. 8, pp. 3694–3711, Oct. 2011.

[6] L. L. Yang, "Signal detection in antenna-hopping space-division multiple-access systems with space-shift keying modulation," *IEEE Trans. Signal Process.*, vol. 60, no. 1, pp. 351–366, Jan. 2012.

[7] D. Tse and P. Viswanath, *Fundamentals of Wireless Communications*. Cambridge, U.K.: Cambridge Univ. Press, 2005.

[8] C. Shepard *et al.*, "Argos: Practical many-antenna base stations," in *Proc. ACM Int. Conf. MobiCom*, Istanbul, Turkey, Aug. 2012, pp. 53–64.

[9] H. Q. Ngo, E. G. Larsson, and T. L. Marzetta, "Energy and spectral efficiency of very large multiuser MIMO systems," *IEEE Trans. Commun.*, vol. 61, no. 4, pp. 1436–1449, Apr. 2013.

[10] F. Rusek *et al.*, "Scaling up MIMO: Opportunities and challenges with very large arrays," *IEEE Signal Process. Mag.*, vol. 30, no. 1, pp. 40–60, Jan. 2013.

[11] E. G. Larsson, F. Tufvesson, O. Edfors, and T. L. Marzetta, "Massive MIMO for next generation wireless systems," *IEEE Commun. Mag.*, vol. 52, no. 2, pp. 186–195, Feb. 2014.

[12] R. Y. Mesleh, H. Haas, S. Sinanovic, C. W. Ahn, and S. Yun, "Spatial modulation," *IEEE Trans. Veh. Technol.*, vol. 57, no. 4, pp. 2228–2241, Jul. 2008.

[13] M. Di Renzo, H. Haas, and P. M. Grant, "Spatial modulation for multiple-antenna wireless systems: A survey," *IEEE Commun. Mag.*, vol. 49, no. 12, pp. 182–191, Dec. 2011.

[14] A. Younis *et al.*, "Performance of spatial modulation using measured real-world channels," in *Proc. IEEE VTC*, Sep. 2013, pp. 1–5.

[15] N. Serafimovski *et al.*, "Practical implementation of spatial modulation," *IEEE Trans. Veh. Technol.*, vol. 62, no. 9, pp. 4511–4523, Nov. 2013.

[16] J. Zhang, Y. Wang, L. Ding, and N. Zhang, "Bit error probability of spatial modulation over measured indoor channels," *IEEE Trans. Wireless Commun.*, vol. 13, no. 3, pp. 1380–1387, Mar. 2014.

[17] E. Bjornson, L. Sanguinetti, J. Hoydis, and M. Debbah, "Optimal Design of Energy-Efficient Multi-User MIMO Systems: Is Massive MIMO the Answer?" Mar. 2014. [Online]. Available: http://arxiv.org/abs/1403.6150

[18] S. C. Wang, Y. Z. Li, and J. Wang, "Convex optimization based multiuser detection for uplink large-scale MIMO under low-resolution quantization," in *Proc. IEEE ICC*, Jun. 2014, pp. 4789–4794.

[19] S. C. Wang, Y. Z. Li, and J. Wang, "Multiuser detection for uplink large-scale MIMO under one-bit quantization," in *Proc. IEEE ICC*, Jun. 2014, pp. 4460–4465.

[20] P. Som and A. Chockalingam, "Spatial modulation and space shift keying in single carrier communication," in *Proc. IEEE Intern. Symp. PIMRC*, Sep. 2012, pp. 1962–1967.

[21] F. Kschischang, B. Frey, and H.-A. Loeliger, "Factor graphs and the sum-product algorithm," *IEEE Trans. Inform. Theory*, vol. 47, no. 2, pp. 498–519, Feb. 2001.

[22] S. Wu *et al.*, "Expectation propagation based iterative groupwise detection for large-scale multiuser MIMO-OFDM systems," in *Proc. IEEE WCNC*, Apr. 2014, pp. 236–241.

[23] S. Rangan, A. Fletcher, V. Goyal, and P. Schniter, "Hybrid generalized approximate message passing with applications to structured sparsity," in *Proc. IEEE ISIT*, Jul. 2012, pp. 1236–1240, Full version: arXiv:1111.2581 [cs.IT]. [Online]. Available: http://arxiv.org/pdf/1111.2581v2.pdf

[24] A. Mezghani and J. A. Nossek, "Belief propagation based MIMO detection operating on quantized channel output," in *Proc. IEEE ISIT*, Jun. 2010, pp. 2113–2117.
[25] U. S. Kamilov, V. K. Goyal, and S. Rangan, "Message-passing dequantization with application to compressed sensing," *IEEE Trans. Signal Process.*, vol. 60, no. 12, pp. 6270–6281, Dec. 2012.
[26] S. Rangan, "Generalized approximate message passing for estimation with random linear mixing," in *Proc. IEEE ISIT*, Jul. 2011, pp. 2168–2172, Full version: arXiv:1010.5141 [cs.IT]. [Online]. Available: http://arxiv.org/pdf/1010.5141v2.pdf
[27] F. Krzakala, M. Mezard, F. Sausset, Y. Sun, and L. Zdeborova, "Probabilistic reconstruction in compressed sensing: Algorithms, phase diagrams, and threshold achieving matrices," *J. Stat. Mech., Theory Exp.*, vol. 2012, 2012, Art. ID. P08009.
[28] J. H. C. Heuvel, J. P. Linnartz, P. G. M. Baltus, and D. Cabric, "Full MIMO spatial filtering approach for dynamic range reduction in wideband cognitive radios," *IEEE Trans. Circuits Syst. I, Reg. Papers*, vol. 59, no. 11, pp. 2761–2773, Nov. 2012.
[29] A. Mezghani, M. S. Khoufi, and J. A. Nossek, "A modified MMSE receiver for quantized MIMO systems," in *Proc. Int. ITG Workshop Smart Antennas*, Feb. 2007.
[30] J. Proakis, *Digital Communication*, 4th ed. New York, NY, USA: McGraw-Hill, 2008, pp. 113–125.
[31] J. Max, "Quantizing for minimum distortion," *IRE Trans. Inf. Theory*, vol. 6, no. 1, pp. 7–12, Mar. 1960.
[32] S. Sesla, I. Toufik, and M. Baker, *LTE—The UMTS Long Term Evolution: From Theory to Practice*, 2nd ed. Hoboken, NJ, USA: Wiley, 2011.
[33] I. Barhumi, G. Leus, and M. Moonen, "Optimal training design for MIMO-OFDM systems in mobile wireless channels," *IEEE Trans. Signal Process.*, vol. 51, no. 6, pp. 1615–1624, Jun. 2003.
[34] Q. Guo, L. Ping, and D. Huang, "A low-complexity iterative channel estimation and detection technique for doubly selective channels," *IEEE Trans. Wirless Commun.*, vol. 8, no. 8, pp. 4340–4349, Aug. 2009.
[35] K. B. Petersen and M. S. Pedersen, *The Matrix Cookbook*. Kgs. Lyngby, Denmark: Tech. Univ. Denmark, 2006. [Online]. Available: http://www.mit.edu/wingated/stuff_i_use/matrix_cookbook.pdf
[36] Y. C. Eldar and G. Kutyniok, *Compressed Sensing: Theory and Applications*. Cambridge, U.K.: Cambridge Univ. Press, 2012.
[37] M. K. Varanasi, "Group detection for synchronous Gaussian code-division multiple-access channels," *IEEE Trans. Inf. Theory*, vol. 41, no. 4, pp. 1083–1096, Jul. 1995.
[38] M. Grossmann and C. Schneider, "Groupwise frequency domain multiuser MMSE turbo equalization for single carrier block transmission over spatially correlated channels," *IEEE J. Sel. Areas Commun.*, vol. 5, no. 8, pp. 1548–1562, Dec. 2011.
[39] Z. Zhang and B. D. Rao, "Sparse signal recovery with temporally correlated source vectors using sparse Bayesian learning," *IEEE Trans. Signal Process.*, vol. 5, no. 5, pp. 912–926, Sep. 2011.
[40] A. Adhikary, J. Nam, J.-Y. Ahn, and G. Caire, "Joint spatial division and multiplexing: The large-scale array regime," *IEEE Trans. Inf. Theory*, vol. 59, no. 10, pp. 6441–6463, Oct. 2013.
[41] W. Bajwa, J. Haupt, A. Sayeed, and R. Nowak, "Compressed channel sensing: A new approach to estimating sparse multipath channels," *Proc. IEEE*, vol. 98, no. 6, pp. 1058–1076, Jun. 2010.
[42] M. Di Renzo, D. De Leonardis, F. Graziosi, and H. Haas, "Space shift keying (SSK-) MIMO with practical channel estimates," *IEEE Trans. Commun.*, vol. 60, no. 4, pp. 998–1012, Apr. 2012.
[43] E. Basar, U. Aygolu, E. Panayirci, and H. Poor, "Performance of spatial modulation in the presence of channel estimation errors," *IEEE Commun. Lett.*, vol. 16, no. 2, pp. 176–179, Feb. 2012.

Shengchu Wang received the B.S. and M.S. degrees in electronic engineering from Beijing Institute of Technology (BIT) and Tsinghua University, Beijing, China, in 2008 and 2011 respectively. Now, he is pursuing the Ph.D. degree at Tsinghua University. His research focuses on designing baseband algorithms for massive MIMO based on compressed sensing and convex optimization.

Yunzhou Li (M'06) received the Ph.D. degree from Tsinghua University in 2004. Nowadays, he is an Associate Professor at Tsinghua University. He mainly focus on signal processing technologies in wireless and mobile communications, including spatial-time signal processing, channel estimation, multi-user detection, and synchronization algorithms for CDMA/OFDM system. He is also interested in analysis, optimization design and enhancement of cellular system and WLAN.

Jing Wang (M'99) received the B.S. and M.S. degrees in electronic engineering from Tsinghua University, Beijing, China, in 1983 and 1986, respectively. He has been on the Faculty at Tsinghua University since 1986. He is currently a Professor at the School of Information Science and Technology. He serves as the Vice Director of the Tsinghua National Lab for Information Science and Technology. His research interests are in the area of wireless communications, including transmission and networking technologies of 4G/B4G. He has published more than 150 conference and journal papers.